


Doctoral Dissertation
Doctoral Program in Bioengineering and Medical-Surgical Sciences (34^{th} cycle)

Development of innovative techniques for autonomous diagnosis of heart-rhythm to be implemented in automated external defibrillators

Jacopo Ferretti
* * * * *

Supervisor
Prof. Eros Pasero, Supervisor
Prof. Alberto Audenino, Co-supervisor

Politecnico di Torino

I hereby declare that, the contents and organization of this dissertation constitute my own original work and does not compromise in any way the rights of third parties, including those relating to the security of personal data.

. . . . . .

Jacopo Ferretti

Turin, October 6, 2022

Summary

According to the World Health Organization, Cardio-Vascular Diseases (CVDs) are the worldwide' leading cause of death. Although not even remotely accounting for the same amount of deaths, a particularly pernicious condition associated with the most common CVDs is Sudden Cardiac Arrest (SCA). SCA is a deadly condition in which the heart unexpectedly stops beating in a functional manner, thus effectively stopping the patient's blood flow. When this happens the patient can only survive if the blood's flow is promptly restored by restarting the heart's activity, e.g. with defibrillation; or by artificially forcing the flow, e.g. with Cardio-Pulmonary Resuscitation (CPR). What makes especially deadly SCA, besides requiring immediate action, is that the underlying causes can remain silent until the fatal event. Nowadays, the only effective weapons to fight SCA are preventive screenings, and a readily available Automated External Defibrillators (AED). An AED is a defibrillator that automates most of the defibrillation process, including formulating a diagnosis on the patient; thus it can be used by layman after a basic training.

Thanks to the continuous advancements in technology, smart and wearable devices are rapidly gaining a place in every home; and with the current trend of integrating more and more sensors, such devices offer an interesting prospective in the healthcare field. As a matter of fact, devices capable of acquiring various vital parameters such as the Electrocardiogram (ECG) or the photoplethysmogram (PPG) are already a reality, albeit still not so common. Being able to frequently monitor the heart's condition by means of such parameters could open new scenarios in the fight to CVDs. Besides offering an effective and practical way on spotting early signs of CVDs, or monitoring an existing condition; these devices leave open some interrogatives on the huge amount of data they produce and the elaboration it will require. In fact, finding a reliable algorithm capable of recognizing arrhythmia is still an open problem.

Born from the joint collaboration of Università degli studi di Toirino, Politecnico di Torino, and Elpro SRL; this doctorate dissertation aims to tackle the abovementioned problems to provide a contribution towards a better understanding, and perhaps a small step in finding some solutions.

After a brief introduction on the challenges and aspects related to AEDs and ECG in general on Chapter 1, a novel series of wearable devices is presented on

Chapter 2. What follows then is an attempt on generalizing heart rhythm recognition with the use of neural networks on Chapter 3. Finally, Chapter 4 and Chapter 5 deal specifically with the SCA problem respectively in terms of defining a better algorithm for shockable rhythm recognition and develop a consumer-grade fully-fledged AED that implements the aforementioned algorithm.

Contents

List of Tables

List of Figures

Chapter 1

An overview on Electrocardiography, Sudden Cardiac Arrest, and defibrillators

Sudden Cardiac Arrest (SCA) is a condition in which the heart suddenly and unexpectedly stops beating in a functional manner, thus effectively stopping the blood flow. During such an event the patient only has a chance of survival if the blood flow is restored as soon as possible by: restarting the heart's activity, e.g. via defibrillation; or by artificially forcing the flow, e.g. with cardio pulmonary resuscitation (CPR). Delays in restoring the blood flow can be fatal, and even in the best case scenario the patient risks a series of complications due to hypoxia[1].

Despite SCA is usually the result of other cardiac diseases, it is still extremely difficult to prevent because the causes are usually asymptomatic until the fatal event. It is, in fact, fairly common to occur in young adults with no previous history of heart diseases, and even athletes [2, 3, 4]. Indeed, it is now common practice -or even required by law in some countries (e.g. Italy)- for amateurs and professional athletes to do annual cardiac screenings to possibly avoid or reduce chances of SCA.

Typically, a routine check on the heart involves analyzing measurements taken with Electrocardiography, and in some cases Echocardiography. In Electrocardiography, two or more (up to ten) electrodes are placed in specific part of the body to register the difference in potential caused by the heart's activation. Plotting the registered voltage versus time gives the electrocardiogram (ECG), which contains detailed information about the heart's activity, and thus it's possible to assert its status. In Echocardiography, instead, ultrasounds are used to create a live image of the heart and its surrounding. The resulting video can be used to assert anomalies in the heart structure or in its movement. Unlike ECG, Echocardiography can give morphological information about the heart, but ECG can give precise timing data. However, Echocardiography is expensive and difficult to perform limiting its use

only in cases where there is already a suspect of a heart condition. ECG, on the contrary, it's relatively easy to perform, it's also faster, cheaper, and it require less sophisticated hardware that can be integrated in mobile or even wearable devices, allowing therefore a mean of monitoring the heart status during everyday activities.

As a matter of fact, during the last few years there has been a growing trend on the market of low-cost devices capable of acquiring ECG targeted at ordinary (non-physician) people. Even some popular smart-watches, like the Apple Watch (Figure 1.1a)[5], are now integrating a built-in two-leads ECG. The capillary diffusion of ECG capable devices can eventually lead to a better and more timely diagnosis of heart diseases, and hopefully to the reduction of SCA deaths as a consequence. However, there is still an open problem regarding the interpretation of this kind of data in the huge amount that is produced. It would be unrealistic to think that every ECG acquisition would be investigated by a cardiologist. On the other hand, a fully automated system would require a non-negligible degree of complexity that not even big companies like Apple are ready to provide. In fact, despite being able not only to register ECG, but also recognizing atrial fibrillation, the Apple Watch is not certified as a medical device and it cannot provide diagnosis[6]. It can only warn the user that its heart-beat might contain anomalies, and thus they should contact a cardiologist. Basically, in this hybrid approach the smart-device detects anomalies and then the cardiologist formulates a diagnosis. Therefore, those devices are not aimed at becoming a sort of substitution to the cardiologist, but a reliable companion capable of spotting early signs of certain diseases that would have remained undiscovered otherwise. Given how early-stage is the adoption of such technology in consumer devices, there is still a huge margin of improvement. For instance: most devices are only capable of recording two-leads ECG, whilst only a handful can record six-leads ECG (Figure 1.1b)[7]. Furthermore, most of them are only capable of asserting atrial fibrillation, ignoring any other form of rhythm anomaly that might be recognized in ECGs. In particular, automated rhythm recognition is what makes this kind of devices so interesting and practical in detecting heart diseases.

(a) Apple Watch.

(b) AliveCore KardiaMobile 6L.

Figure 1.1: Example of consumer products with ECG recording capabilities.

Albeit the main topic of this thesis is an algorithm capable of recognizing SCA, it is undeniable the impact that ECG capable wearable devices could have on spotting early signs of heart diseases, which ultimately can lead on prevention of SCA. Since the two arguments are closely related we decided that would be of great interest to include in this study the design of an ECG wrist-watch united with a neural algorithm capable of recognizing different kinds of arrhythmia starting from a single lead ECG signal. These topics will be treated on Chapters 2 and 3 respectively. The SCA algorithm, instead, is presented on Chapter 4, while the defibrillator on which the algorithm is implemented is treated on 5. However, there are a few recurring concepts to address before ending this brief introduction, which are: the Electrocardiogram signal, the Sudden Cardiac Arrest, and finally defibrillators.

1.1 Electrocardiography

In a formal definition, Electrocardiography is the procedure in which the heart's electrical activity is recorded in the form of an electrocardiogram (ECG or also known as EKG) using electrodes placed on the patient's skin. Each contraction of the heart follows a fairly precise pattern of depolarization and re-polarization of the cells through the conduction of a pulse known as *action potential*. This pattern originates from the *pacemaker cells* in the *sinoatrial node*, which are the responsible for every heartbeat's origin. The pulse moves from the *sinoatrial node* through the atria to the *atrioventricular node*. After which it continues through the *bundle of his* where it separates in the *left and right bundle branches*, which are respectively responsible of the left and right ventricle activation. Finally, the pulse ends in the *Purkinje fibers*, which are the *branches* terminations. The action potential movement through this intricate net of conducting fibers (shown in Figure 1.2a)

produces a difference in potential that can be sensed through electrodes placed on the skin. The electrocardiogram is the plot of such differences of potential versus the time.

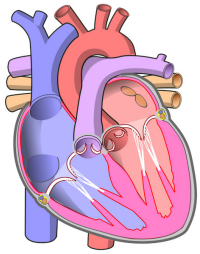

(a) Diagram of the human heart[8].

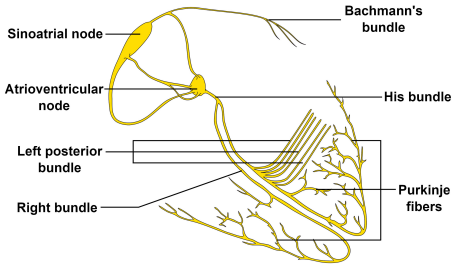

(b) Conduction system of the human heart[9].

Figure 1.2: The human heart and its pulse conduction system.

Depending on where on the patient the electrodes are placed the ECG has different characteristic waveforms that can be interpreted by cardiologists. The signal produced by the difference between different electrodes is called lead (or rarely derivation), and the number of leads is usually different by the number of electrodes. The simplest configuration for an ECG is the single lead ECG, in which the plot only consists of the potential difference between two electrodes. However, the most common analysis use 10 electrodes for a twelve leads ECG, or 4 electrodes which produce six leads ECG. Single lead ECG are commonly taken from limb to limb, usually from the arms, because it's the most comfortable way of acquiring it without having to take off clothes. Six leads ECG are instead taken placing the electrodes on all the limbs. However, one of the electrodes (the right leg one) is used as a common reference in order to reduce the noise, and therefore is not producing a signal. The leads are then derived according to the Einthoven's triangle[10, 11], with the help of a virtual ground known as Wilson's central terminal (produced by the average of the limbs signals), as shown in Figure 1.3a. Adding six more electrodes to the chest of the patient according to Figure 1.3b, it is possible to derive twelve leads ECG[12].

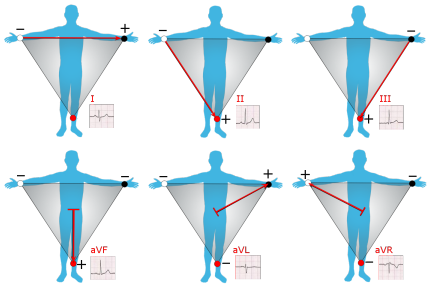

(a) Einthoven's triangle, and the six resulting leads[13].

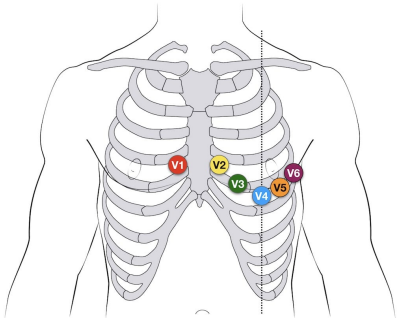

(b) Precordial electrodes placement[14].

Figure 1.3: ECG electrodes placement.

Each lead highlights different aspects of the heartbeat, and thus they all have a different interpretation. However, even a single lead signal can be enough to extract a vast amount of information about the heart's condition. For instance, Figure 1.4 shows a single heartbeat as seen in lead I. In this image there are highlighted the various waves that compose a single heartbeat. In particular, it is fairly trivial to divide it in three different entities, each related to distinct phases of the heart's activation [15, 12].

- The **P wave**, which represents atrial depolarization. In this phase, the action potential spreads from the sinoatrial node to the atrioventricular node contracting the atria.
- The **QRS complex**, which represents the rapid depolarization of the ventricles. During this phase the action potential diffuses through the bundle branches contracting from top to bottom both ventricles.
- The **T wave** represents ventricular re-polarization after the contraction. At the end of this final phase the ventricles can be stimulated again.

Alterations on length or shape of these macro-elements are usually correlated to some functional alteration of the heart.

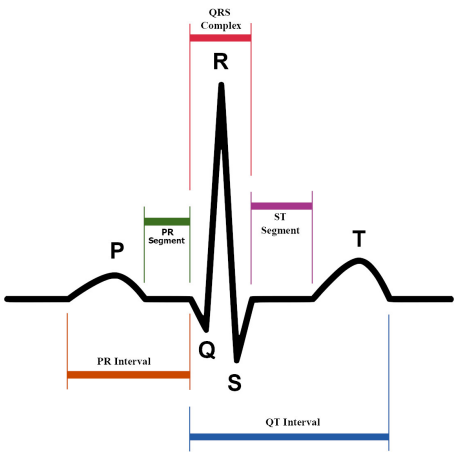

Figure 1.4: ECG of a single heartbeat[16].

1.2 Suddeen Cardiac Arrest

Sudden Cardiac Arrest (SCA) is a condition in which the heart suddenly and unexpectedly stops beating in an functional manner, thus effectively stopping the blood flow. Under this critical condition the patient will die in the course of just a few minutes as their organs deplete all available oxygen contained in the blood. Albeit cerebral neurons in normal conditions can resist up to 20 minutes in a low oxygen environment, cerebral recovery from more than 5 minutes of cardiac arrest is hampered by complex secondary derangement of multiple organ systems after re-perfusion [17] (effect known as post-resuscitation syndrome). Therefore, it is imperative not only for the patient's survival, but also for their well-being, that the blood flow is restored as soon as possible by either restoring the heart's normal functioning, or forcing it externally [1].

Causes and mechanisms

There are various causes that can lead to SCA, of both cardiac and non-cardiac nature. It is out of the scope of this brief introduction to treat them all in detail. However, there is a common element among the causes and it's the alteration of the electrical activity and/or response of the heart tissue. This usually manifests with a variation of the preferential path for the action potential's conduction (see Figure 1.2b), or the cellular response at its passage. This critical alteration results in loss of synchrony between the heart's cells, which then start to produce ineffective contractions thus stopping the blood's flow.

SCA can manifest in different rhythm alterations. However, the most common and characteristic are *Ventricular Tachycardia* (VT) and *Ventricular Fibrillation* (VF).

Ventricular Tachycardia (VT) is a rhythm alteration in which the ventricles, regardless of the atria, contracts multiple times in rapid succession, usually with a rather high frequency (above $100bpm$, up to $250bpm$) [18, 19]. Depending on the gravity of the causes this condition can last a few seconds, not causing a serious risk for the patient; or persist for more drastically reducing the cardiac output, with the additional risk of degenerating into VF.

VT is usually caused when the cardiac pulse is not generated in the sinoatrial node, but instead in other stimulated ventricular cell. Another mechanism that can cause VT is the presence of non-conductive scar tissue on the heart which may cause the formation of a re-entrance circuit. Therefore, once the pulse is generated, it starts circulating around the heart causing spontaneous and uncontrolled contractions.

Depending on its duration or morphology VT has different classifications. When three or more premature ventricular contractions happen within a maximum duration of 30 seconds, the VT is classified as *Non-sustained* [20], otherwise if the events extends to more than 30 seconds of duration it's a case of *Sustained VT* [21]. Depending on the ECG shape it is also possible to define: *Monomorphic VT* [22] (or mono-phasic) when all ventricular beats have the same shape, *Biphasic VT* when the QRS complexes alternates from beat to beat, or *Poly-phasic VT* [23] in the case where all ventricular beats are different from each other.

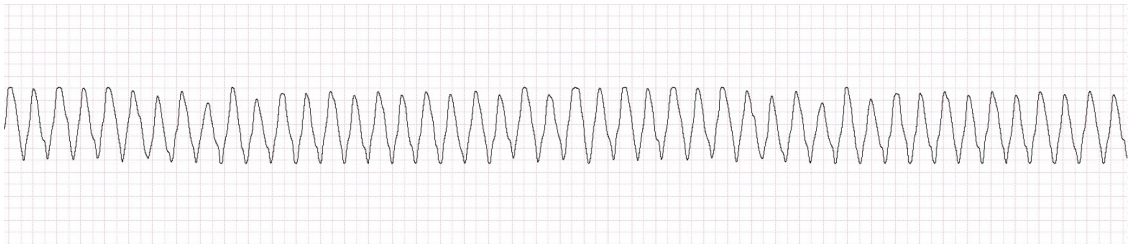

Figure 1.5: ECG of a Ventricular Tachycardia. Acquired using the AED proposed in Chapter 5 and a patient simulator. The ECG is plotted with $2mm/mV$ and $5mm/sec$ settings.

Ventricular Fibrillation (VF) is a rhythm dominated by an uncoordinated and chaotic electrical activity of the heart. During VF the ventricles are quivering, contracting in a completely ineffective manner[24, 25]. VF is a deadly condition which has to be treated as soon as possible to avoid death. There are multiple causes for VF occurrence, but the most common is the result of the damage provoked by cardiac disease. It is extremely common as a result of an underlying ischemic heart disease. Other causes can be related to: drugs, and drugs overdose, extreme electro-chemical imbalances (especially hyperkalemia or hypokalemia), damages on the tissues, etc.

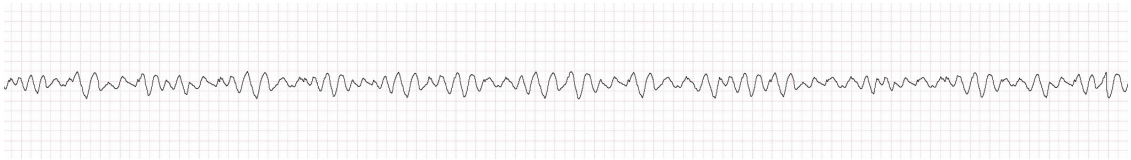

Figure 1.6: ECG of a Ventricular Fibrillation. Acquired using the AED proposed in Chapter 5 and a patient simulator. The ECG is plotted with $2mm/mV$ and $5mm/sec$ settings.

Diagnosis

The main symptoms of SCA are absence of pulse and consciousness. However, the diagnosis can only be formulated with the ECG analysis. In ECGs, Ventricular Tachycardia usually appears as a rapid repetition of wide and tall peaks, whilst the Ventricular Fibrillation follows a chaotic pattern.

Treatment

Although VT can effectively be treated with cardioversion, medication, and surgery; defibrillation remain the preferable option. Good timing is vital to avoid further damage and/or the degeneration to VF [26].

Things are different for VF, which is only treatable with immediate defibrillation.

1.3 Defibrillators

A defibrillator is an electrical medical device capable of releasing a therapeutic dose of electric energy (called defibrillation) into a patient who is suffering from certain conditions like Sudden Cardiac Arrest (SCA). An overview of the mechanisms involved in a defibrillation is in [27]. Defibrillators can be divided in two main macro-groups depending on their intended use: internal (or implantable) defibrillators, which are surgically implanted into a high risk patient who needs defibrillation frequently; or external defibrillators, which are devices commonly used in emergencies. Internal defibrillators are out of the scope of this thesis, so they will not be treated with more detail.

An external defibrillator is a portable device that usually incorporates different vital parameters acquisition systems and a display to monitor them. Among the vital parameter that a defibrillator can acquire from a patient, the ECG is the most important, and therefore always present. A trained physician can use a defibrillator on a patient to both diagnose SCA interpreting the ECG, and treat it with defibrillation. Among the external defibrillators, there is a specific class which

is particularly interesting for the purpose of this thesis, which are the Automated External Defibrillators (AED).

An AED is a defibrillator capable of autonomously recognizing ECG signals related to SCA and perform defibrillation when required. In other words, and AED is a defibrillator that only requires a basic training to be operated, and therefore it can be used by non-physicians, widening the use scenario of defibrillators outside the hospitals. The need of AEDs arose by the deadliness of SCA, which is the result of the combination between an immediate need for assistance with the possibility of happening at any time. Without intervention the person can die within a few minutes. Even in the best case scenario, it is highly improbable that a medical team is able to arrive in this short time, and thus the patient's life is usually in the bystander's hands.

An AED is a device designed to be used by lay persons, without a medical background. Therefore they have to be extremely easy to use, resilient to errors, and ideally they shouldn't rely on the operator if not for the most basic actions. A typical AED has both audible and visible instruction for its use, which guide the user through the resuscitation phases. A typical operation of an AED follows these steps:

1 The AED will give preliminary instructions such as to call the emergency number, and to stay calm.

2 Instruct the operator on how to apply the electrodes on the patient and wait until they are placed.

3 Analyze the patient's ECG to decide whether they need a defibrillation or not. In the negative case step 4 is not performed.

4 Charge the defibrillation circuit and instruct the user on how to release the discharge (usually with a button).

5 Guide the user into performing Cardio Pulmonary Resuscitation (CPR).

6 Repeat the cycle from step 3 until an emergency squad arrives or the patient regain consciousness.

The above passages are the synthesis of the American Heart Association guidelines [28]. There may be subtle differences between different brands of AEDs, however the key concept is always the same: make any person able to help a victim of SCA in the matter of seconds instead of minutes.

Chapter 2

Wearable ECG devices

As briefly discussed in the introduction, wearable devices have a huge unused potential in preventing diseases by giving a mean of self-checkup to a wide consumer audience. The widespread application of these checks could be used in spotting early signs of diseases, to monitor the state of a known condition, or just to assert the well-being of a person. It is undeniable how the advent of smart devices revolutionized modern society. Smartphones, smartwatches, and all sort of Internet of Things (IoT) devices flooded our lives with many kind of sensors that could have a major impact on people's health. For instance: accelerometers can be used to detect falls, which can be a life-saving feature for the elderly [29]; cameras or custom-made sensors can be used to assert a driver's state of attention to avoid accidents [30]; optical heart-rate monitors can be used to keep track of the cardio-pulmonary response during exercise [31], or to monitor sleep quality [32]; and many more. The applications are of various nature: some exploiting sensors commonly available in smartphones or similar devices, some using brand-new hardware targeted to specific applications.

In this dissertation the focus is on ECG capable devices, which require a fairly simple hardware that could be introduced in many consumer devices such as smartwatches or smartphones. Having close at hand a device capable of acquiring an ECG can drastically facilitate the monitoring of patient at risk by eliminating the need of going to hospitals. For example: a cardiologist can assert the status of a patient at distance just by requesting an acquisition. Furthermore, frequent ECG acquisitions on demand could be better suited on spotting sporadic events than holters. In fact, holters use is limited on cases where there is already a suspect of some sort of arrhythmia, can only monitor the patient for a finite amount of time [33] (typically 48 hours), and with the associated discomfort of having to wear a device attached on the chest. On the other hand, introducing ECG capabilities on a consumer device has the advantage of allowing a permanent, although discontinuous, tracking of the ECG. Moreover, it can be used to promptly check the heart's status when the patient is feeling transitory discomforts such as: palpitations, short

of breath, chest pain, etc; which could only persist for a brief amount of time, not sufficient to book an appointment with a specialist.

In the market there are already available some portable ECG. The most notorious case is probably the Apple Watch [5], which is incorporating an ECG circuit since its 4th generation (also called Series 4) in 2019. The Apple Watch (Figure 2.1a) uses the back of its metal body chassis as the first electrode, and the digital crown as the second. Therefore, its use is limited to one lead ECGs, which is good enough to incorporate an atrial fibrillation detection algorithm. However, the measurements are restricted to lead I acquisitions with a fixed duration of 30 seconds, and can only be viewed and shared when paired with an Apple iPhone.

(a) Apple Watch.

(b) D-HEART PORTABLE ECG DEVICE.

(c) AliveCore Kardia.

(d) AliveCore Kardia 6L.

Figure 2.1: Some example of consumer products with ECG capabilities.

The AliveCore KardiaMobile [7] (Figure 2.1c), and the new generation KardiaMobile 6L [34] (Figure 2.1d) are two other examples of consumer ECG device. Unlike the Apple Watch it relies on a custom stick-like form factor, which only serves as an electrocardiograph. KardiaMobile 6L has three electrodes allowing both single lead and six lead acquisitions: two of them are on the front, meant to be touched with the left and right hand respectively; and one is on the back, which

should be in contact with the left leg. It needs a smartphone in order to work, to which it connects via Bluetooth using its dedicated app; and it can record an ECG of variable length from 30 seconds up to 5 minutes. The app shows the ECG in real time, and after the acquisition it provides a simple rhythm evaluation. However it can only recognize: atrial fibrillation, bradycardia, tachycardia, and normal heart rhythm.

Finally, the D-Heart portable ECG device [35] (Figure 2.1b) is a semi-professional ECG acquisition system, which is capable of 8 lead and asynchronous 12 lead acquisitions. Unlike the Apple Watch and the AliveCore KardiaMobile, the D-Heart has a holter-like form factor that trades off portability and comfort for the sake of better acquisitions. In fact, it uses six disposable electrodes positioned on the chest: three used in the Einthoven's configuration, two on the center of the chest, and the last is positioned in one of the precordial positions. By moving the last one it is possible to acquire all 12 derivations, albeit not at the same time for obvious reasons. The final result is then available on a smartphone connected via Bluetooth. The downside of this approach is that it needs training on placing the electrodes in their correct positions. Indeed, even a few centimeters can make a huge difference on the placement of precordial electrodes since there is far less margin than those placed on the limbs. However, this is a viable choice for professionals who needs to visit patients without the need of moving bulky electrocardiographs, or for patients with particular conditions who need a more in-depth monitoring of their heart.

2.1 Case study: ECG Watch

ECG Watch [36, 37, 38] (Figure 2.2) is a device developed in the Neuronica Lab. As the name suggests, it is a wrist-worn electrocardiograph and it's capable of single lead acquisitions using two electrodes: one on the front, and one on the back. The one-lead limitation however, does not constrain the user on just lead I acquisitions. In fact, by placing one of the electrodes on the left thigh it is possible to acquire lead II or lead III ECGs if the other electrode is in contact with the right or left hand respectively [11]. The acquisitions are controlled using a smartphone app, connected to ECG Watch via Bluetooth 2.0. Using the app it is possible to choose between ten or twenty seconds acquisitions and, once data is collected, it is possible to inspect the ECG as well as saving or sharing it. Just like the Apple Watch, and the AliveCore KardiaMobile, the ECG Watch application has an atrial fibrillation recognition algorithm. However, unlike the device seen so far, ECG Watch was designed to be more open and research-oriented. Therefore, it is possible to export raw data in a clear CSV format so that it can be used for further analysis or to fill a database.

Figure 2.2: ECG Watch.

2.1.1 Hardware

Figure 2.3 contains a schematic representation of ECG Watch's hardware. The device's brain is a Texas Instruments MSP430 micro-controller [39], which is responsible of acquiring the ECG signal as well as controlling the Bluetooth 2.0 module. The analog front-end is a circuit designed to adapt the ECG signal, which is a differential voltage that hardly exceeds a few *millivolts*, to the Analog-to-Digital Converter (ADC) of the micro-controller. Finally, the device is powered by a single LiPo battery that can be recharged using a USB connector type micro-B.

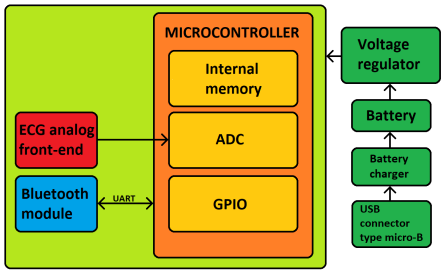

Figure 2.3: ECG Watch block diagram.

The analog front-end, shown in Figure 2.4, can be divided in four different sections (stages). Starting from the left, th first stage (red box) consists of the electrodes connectors and two current limiting resistors, which are required in case of failure to limit the current that may flow in the user. The second stage (orange box) contain a high pass filter which has the double task of removing the unknown DC component of the input signal among very low frequencies (below $100mHz$), and to apply a known DC bias: $VRef$ (indicated simply as Ref in Figure 2.4). $Vref$ is obtained by halving the system voltage supply of $3.3V$ using a resistor divider with a buffer in series to decouple it from the rest of the circuit, as shown in Figure 2.5.

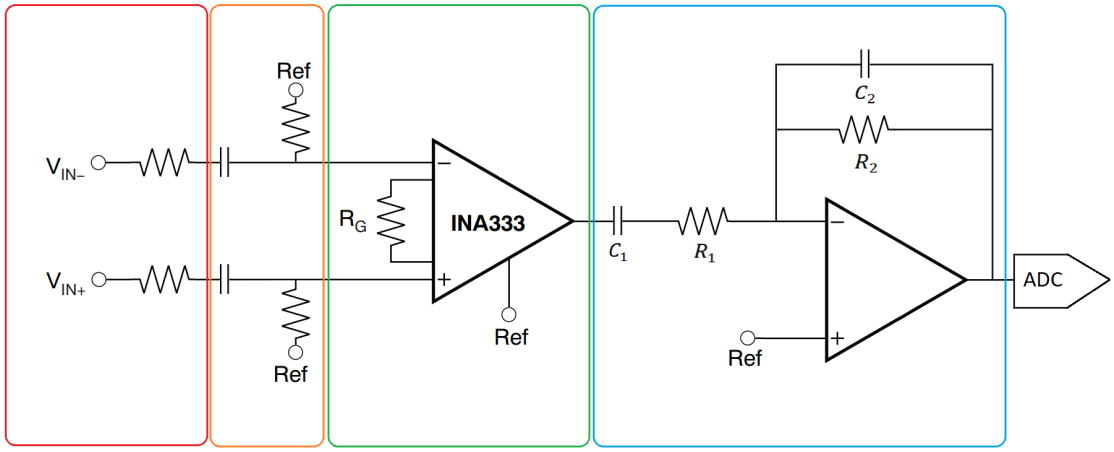

Figure 2.4: ECG Watch analog front-end.

The third stage, highlighted by the green box in Figure 2.4, contains a differential amplifier -the Texas Instruments INA333 [40]. The INA333 is used to transform the differential input signal into a single-ended signal, which is required by the micro-controller's ADC. In this stage there is also an amplification of $40dB$ set by R_G.

The forth and final stage, contained in the blue box, is a first order band-pass active filter, which has the following transfer function:

$$H(S) = -\frac{R_2}{R_1} \cdot \frac{R_1 C_1 s}{R_1 C_1 s + 1} \cdot \frac{1}{R_2 C_2 s + 1} \tag{2.1}$$

The filter has a gain defined by $\frac{R_2}{R_1}$, which is set at $40dB$ for a grand total of $60dB$ amplification with regard to the whole circuit. Finally, since most of the ECG spectrum is concentrated below $70Hz$ [41], the allowed band has been set to $[0.7 - 72]Hz$ by appropriately choosing the positions of the two poles: $-\frac{1}{R_1 C_1}$ and $-\frac{1}{R_2 C_2}$.

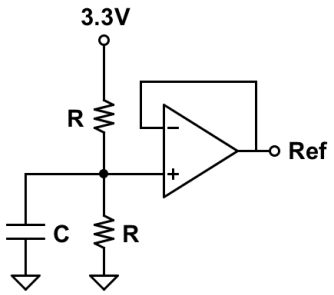

Figure 2.5: ECG Watch Ref circuit.

The final stage of the analog front-end is directly connected to the microcontroller's ADC, which produces a $10bit$ data-stream with a sampling frequency of $1ksps$. Because of the limitation of the Bluetooth 2.0 connection, the resulting data is stored in the internal flash until the end of the acquisition, when it is recovered and sent to the smartphone. The internal flash is sufficient for a little more than 20 seconds, hence the device is configured to work with 10 or 20 seconds fixed-length acquisitions.

Finally, the Bluetooth 2.0 module is a generic HC-06 [42] all-in-one circuit board, chosen for its ease of use and low consumption. The communication is handled through a UART port and a standard AT protocol in which every command is defined by some mnemonic characters followed by their numeric parameters.

Power consumption is always a major concern when dealing with wearable and IoT devices since it lowers the user experience quality. In ECG Watch most of the power is spent in the digital circuit, with an approximate consumption of $30mW$ during the acquisition, and $150mW$ during Bluetooth transmission. On the other hand, the analog circuit only draws $1.5mW$ during its operation. Considering a heavy usage of 50 acquisitions per day and a $120mAh$ battery, the estimated time before needing to recharge it is 8 days.

2.1.2 Performance Evaluations

To assert and evaluate its performance, ECG Watch was compared with a state-of-the-art patient monitor: the General Electrics (GE) B105 [43]. The B105 has been chosen because it is a consolidated monitor widely used in hospitals. Furthermore, having a CE marking it means that it has already passed all the related tests described in the IEC 60601 standards [44], which makes it a reliable choice for comparing ECG Watch.

The tests were performed with the aid of 30 volunteers evenly divided between males and females with an age in the range of 25 and 35 years old with no known cardiac problems. In addition to the volunteers, the patient simulator Fluke ProSim4 was used to evaluate ECG containing rhythm alterations such as atrial fibrillation. The acquisition were taken simultaneously with the B105 attached to the patient using four Silver-Silver Chloride wet electrodes positioned on the limbs; while ECG Watch was used on lead I configuration except in five cases where the signal was not strong enough and thus lead II was used.
Finally, once all data was gathered the post-processing consisted in normalizing and filtering all signals with three different digital filters: a median-based baseline-wonder removal filter, a $50Hz$ notch filter, and a moving average filter to smooth the final results. After filtering, the signals were manually aligned for comparison.

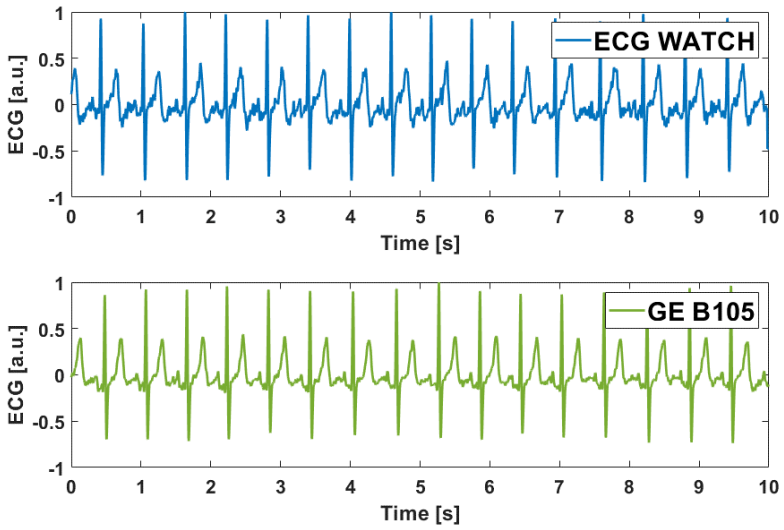

Figure 2.6: Comparison between ECG Watch and GE B105 lead I acquisitions.

In Figure 2.6 there is an example of the results from the acquisition campaign. Despite having a higher noise level, qualitatively speaking ECG Watch's signal do not differ by much from the one obtained by GE B105. However, a quantitative analysis is the only way to rigorously assert the quality of the system. For this purpose it was defined a series of parameters to evaluate comparatively: heart-rate, power spectral density distribution of the signals, signal-to-noise ratio, and finally time-domain difference.

Heart-rate

The heart-rate was evaluated using a Bland-Altman (BA) plot [45, 46]. A BA plot is a technique used to highlight differences between two instruments. Paired acquisitions are plotted in a Cartesian coordinate system where: ordinate represents the difference between a pair of acquisitions, and abscissa represents the mean between them. In this specific case, each point represents a pair of heart-rate estimation, taken from the same signal acquired by ECG Watch and by GE B105.

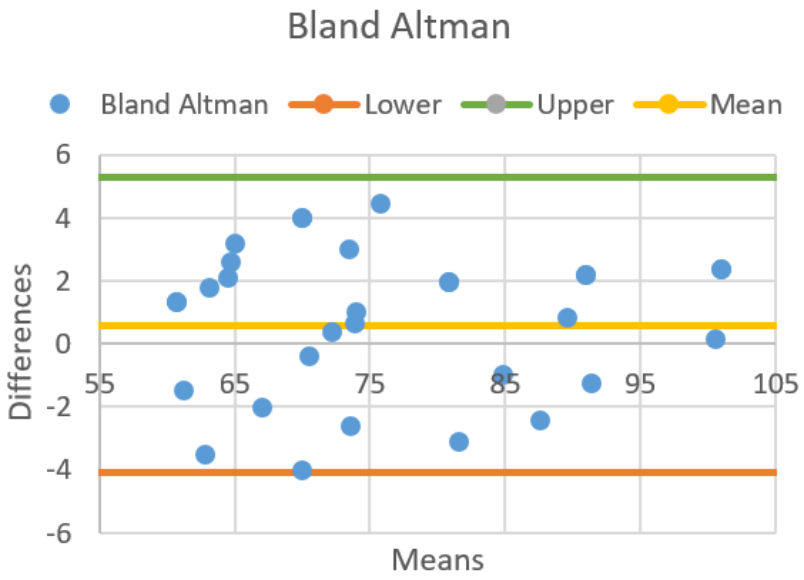

Figure 2.7: Bland-Altman plot of heart-rates estimated from ECG Watch and GE B105. All dimensions are in *bpm*

The BA plot of the heart-rate estimation for ECG Watch and GE B105 is shown in Figure 2.7. From this it emerges that ECG Watch overestimates, on average, the heart-rate by $0.6bpm$, as shown by the mean value highlighted by the yellow line. However, all points are within 5% of the average value meaning measurements are consistent. The upper and lower bound lines highlight the limits of acceptance for this last condition. Finally, cross-correlation (Equation 3.3) between the heart-rate estimation of the two systems were evaluated as a further mean of comparison and it resulted a value of roughly 98.7%, with a mean standard deviation for each subject of $2bpm$. As a result it is possible to say that there are not significant differences between the two devices heart-rate estimations.

Power Spectral Density

The next benchmark to compare ECG Watch and B105 involves frequency domain differences. In particular, Power Spectral Density (PSD) [47] is a function that describes the distribution of power among the frequencies composing a signal. in other words: it provide an insight on the information content of each frequency of the signal. A comparison of the PSD obtained by the two devices can therefore give a quantitative idea on the frequency response quality. There are multiple way of estimating a PSD, but for sake of simplicity the squared discrete Fast Fourier Transform (FFT) module has been chosen:

$$PSD(f) = \frac{(\Delta t)^2}{T} \left| \sum_{n=1}^{N} x_n e^{-iwn\Delta t} \right|^2 \tag{2.2}$$

The results are shown in Figure 2.8 where it's possible to qualitatively compare ECG Watch and GE B105 in the band of $0 - 40Hz$, where the differences are more pronounced.

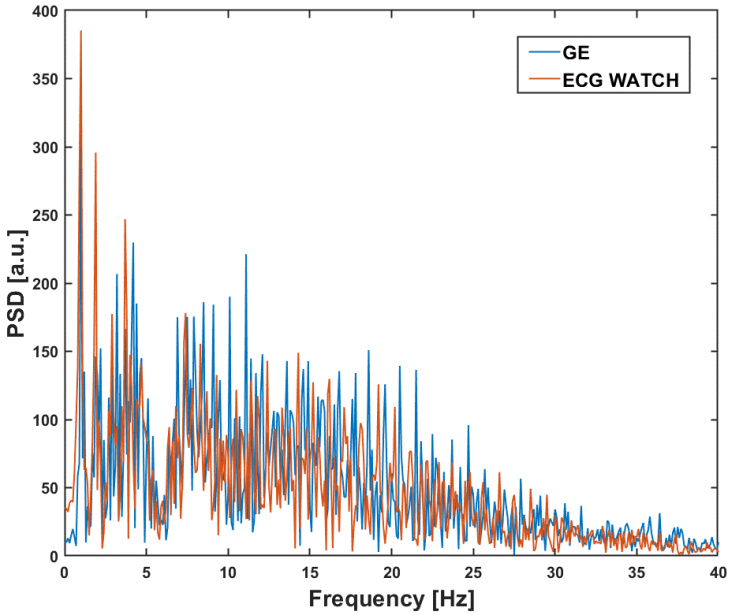

Figure 2.8: PSD plot of ECG Watch and GE B105 signals. The band was restricted to $0 - 40Hz$ in order to highlight differences.

However, despite having a rather artistic impact, not much can be said by simply observing the two signals plot. There is, of course, a certain amount of similarities, however it is just a qualitative comparison. Therefore, an additional parameter was evaluated starting from the PSD: the Cumulative Spectral Power (CSP). The CSP is a cumulative sum of the DSP normalized with regards to the total power. Therefore, the resulting function has a monotone curve contained between 0 and 1, where the numeric value represents the percentage of energy contained up to a specific frequency f. The CSP formula is the following:

$$CSP(f) = \sum_{n=0}^{f} PSD(n) \tag{2.3}$$

Using Equation 2.3 is possible to assert at which frequency the signal contain a certain amount of power, and then compare it between the two measurement systems. The first point of interest is the frequency at which the signal reaches 50%, namely the power median. Then, a bandwidth of 60% around the median has been defined as the second and third frequency of interest. The results are resumed in Table 2.1 in terms of average values for the three frequency of interest for both ECG Watch and GE B105. From this it is possible to say that ECG Watch and GE B105 have a similar content in frequency, even thought the lower bound of ECG Watch bandwidth hints that the spectrum has a wider band.

Table 2.1: CSP Analysis for ECG Watch and GE B105. Frequency of interest.

Device	$f_{20\%}[Hz]$	$f_{50\%}[Hz]$	$f_{80\%}[Hz]$
GE B105	3.9	8.7	15.3
ECG Watch	3.6	8.6	15.3

Signal-to-Noise Ratio

In digital signal processing it is not uncommon to divide an acquired signal into: unmeaningful information, also known as noise; and meaningful information, which is the actual signal. The definition of noise and signal is usually application specific, however a reliable and simple way of doing so is by defining a bandwidth of interest. The data contained in the bandwidth is defined as signal, whilst all remaining is considered noise. The ratio between data inside the bandwidth of interest and outside it is an indication of signal quality.

$$SNR = \frac{P_{Signal}}{P_{Noise}} = \frac{\sum_{n \in B} PSD(n)}{\sum_{n \notin B} PSD(n)} \tag{2.4}$$

In this study the bandwidth was chosen according to IEC 60601-2-27, which defines the monitoring bandwidth in the range of $0.67 - 40Hz$. Furthermore, with regards to Equation 2.4, P_{Signal} and P_{Noise} are respectively the sum of the PSD function evaluated inside and outside the bandwidth of interest B. All the acquired signal's SNR were evaluated and the results are resumed in Table 2.2.

Table 2.2: SNR Analysis for ECG Watch and GE B105.

Device	Mean $[dB]$	Standard Deviation $[dB]$
GE B105	145.7	27
ECG Watch	128.14	10

The results confirm what was qualitatively observed in Figure 2.6, namely that ECG Watch has a noise level slightly higher than GE B105.

Time domain differences

Finally, the last comparison between GE B105 and ECG Watch involved time domain differences. In this test, a single heartbeat is extracted from data in order to evaluate point-to-point discrepancies between the two systems. The heartbeat (Figure 2.9) was manually selected and aligned between the two datasets, then it was normalized, and finally it was compared in pairs.

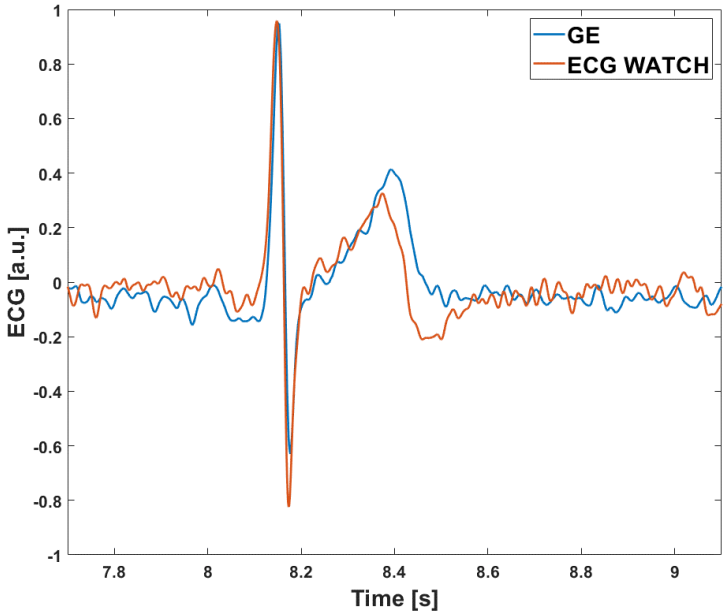

Figure 2.9: The same heartbeat acquired from ECG Watch and GE B105.

Figure 2.9 highlights a qualitative difference between the two acquisition systems: the underlying signal is the same, however ECG Watch has a higher component of noise. On the other hand, Table 2.3 is far more interesting and significant as it highlights that the mean difference is about 2.7%, while the maximum discrepancy between the two signals is over 15%.

Table 2.3: Time domain difference Analysis for ECG Watch and GE B105.

Mean $[a.u.]$	Standard Deviation $[a.u.]$	Max $[a.u.]$
-0.027	0.0931	0.1508

2.2 Vital ECG

The tests described in the last section proved that albeit ECG Watch is not quite on par with a professional certified monitor, its results are not so different either. Furthermore, an indirect effect of the above mentioned tests was the highlight of some technical limitations during the extended use of the device such: as not knowing the battery state of charge, the Bluetooth 2.0 protocol, the overall device size, and the micro-controller performances. Because of the consolidated results obtained with ECG Watch, however, the device was used as a starting point for a new generation of wearable ECG devices: Vital ECG [48].

Vital ECG, shown in Figure 2.10, was designed to overcome some of ECG Watch's weak points as well as to add more sensors in order to obtain more information on the wearer's state. Besides the ECG module, the device also incorporates: a pulse oximeter, a temperature and humidity sensor, and an inertial measurement unit. Vital ECG works with the Bluetooth 4.2 BLE protocol, which requires less power and allow higher data rates. Finally, a battery fuel gauge provides a feedback on the battery state of charge in order to avoid losing data. Despite all the added sensors and functionalities, Vital ECG and ECG Watch share roughly the same dimensions making it possible to use the same case with some minor adaptations.

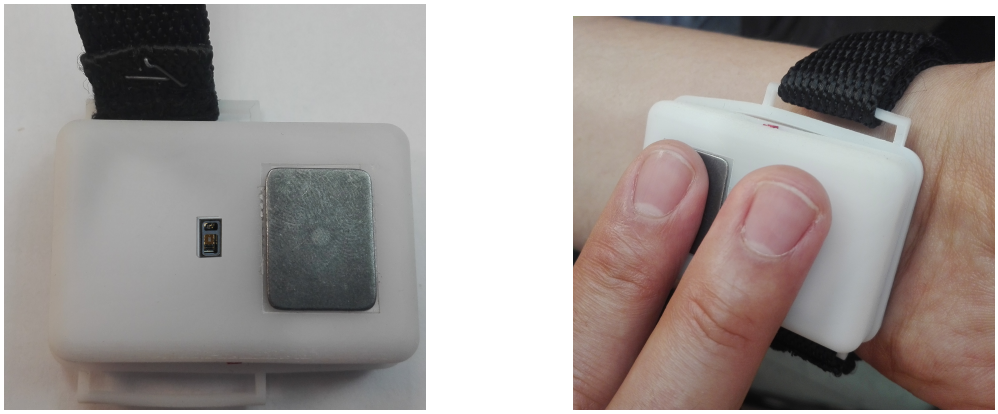

(a) Top view. (b) During acquisition.

Figure 2.10: Vital ECG prototype.

2.2.1 Hardware

Instead of using a Bluetooth module, Vital ECG uses a micro-controller that incorporates the Radio Frequency (RF) circuits. This choice not only reduces the total footprint of the RF circuit, but also improves the communication chain by not requiring anymore an intermediary between the micro-controller and the smartphone.

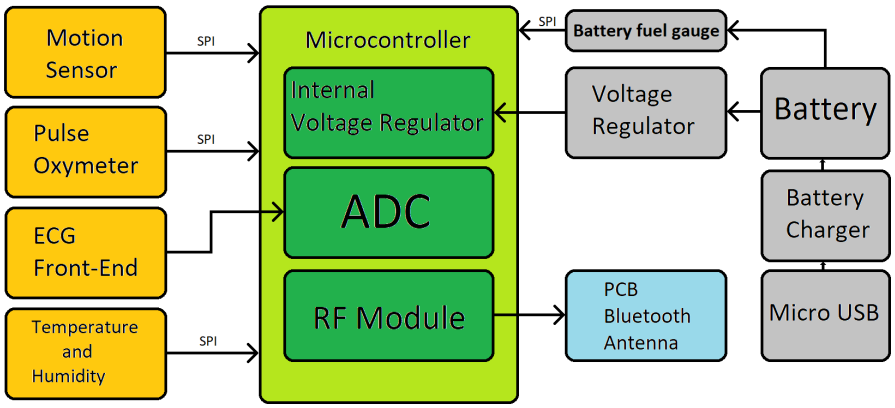

Figure 2.11: Vital ECG block diagram.

Figure 2.11 shows the block diagram of Vital ECG. The chosen micro-controller is a Texas Instruments CC2640R2F [49]. Despite being able of the latest Bluetooth 5.0 connections, the protocol 4.2 was preferred because it required less internal resources allowing better overall performances. Nonetheless, the Bluetooth 4.2 BLE standard was good enough for real time ECG transmission allowing arbitrary length acquisitions.

The Temperature and Humidity sensor incorporated in Vital ECG is a ST HTS221 [50], capable of 16-bit acquisition with a humidity accuracy of 3.5% rH in a range between $20 - 80\%$ rH; and a temperature accuracy of $\pm 5°C$ from 15 to $40°C$.

As Inertial Measurement Unit (IMU), the TDK MPU-9250 [51] was chosen because of its size and relatively low cost. It is a reliable integrated circuit that incorporates a digital motion processor with an internal 16-bit ADC that converts data from: a three-axis accelerometer, a three-axis magnetometer, and a three-axis gyroscope.

Finally, Vital ECG includes a pulse oximeter sensor. A pulse-oximeter is a non invasive sensor capable of measuring the peripheral oxygen saturation (SpO_2) of a person. The core idea behind this technology is that blood has a index of refraction that varies with the oxygen content, hence it is possible to correlate the blood's light absorption with its oxygen content. Therefore, exciting the extremity of a finger, where the capillary vessels are more exposed to outside light sources, with a known wavelength light emitted by a LED it is possible to measure the reflected light and estimate the blood's light absorption. In actual acquisitions, however, two LEDs with different wavelength are employed: one more sensitive to oxygenated hemoglobin, and one more sensitive to de-oxygenated hemoglobin. This allows the estimation of the percentage of oxygenated hemoglobin in the peripheral bloodstream with a simple ratio given by:

$$SpO_2 = \frac{HbO_2}{HbO_2 + Hb} \tag{2.5}$$

where Hb and HbO_2 are respectively the blood's concentration of de-oxygenated and oxygenated hemoglobin.

The pulse oximeter sensor chosen in Vital ECG is a Maxim MAX30102 [52]. The MAX30102 was chosen because it integrates the LEDs and the photo-diodes in a single package along with the related optics and control circuits.

In what regards the ECG circuits there are two major changes from ECG Watch. The first one is that is not relying anymore on AC coupling to eliminate low frequencies, the second one, instead, is that is using wider bandwidth in the filters. The idea behind this choices was to obtain the most accurate reconstruction of the input signal, and then apply digital filters to enhance the results. This allows not only to adjust the filters for different applications, but also to obtain a raw recording of the ECG for research purposes.

The new front-end circuit is shown in Figure 2.12 and it can be divided in two parts: on the left half the first stage containing the differential amplifier and the baseline-wonder filter; and on the right half a second order active low-pass filter composed of a Sallen-Key cell [53].

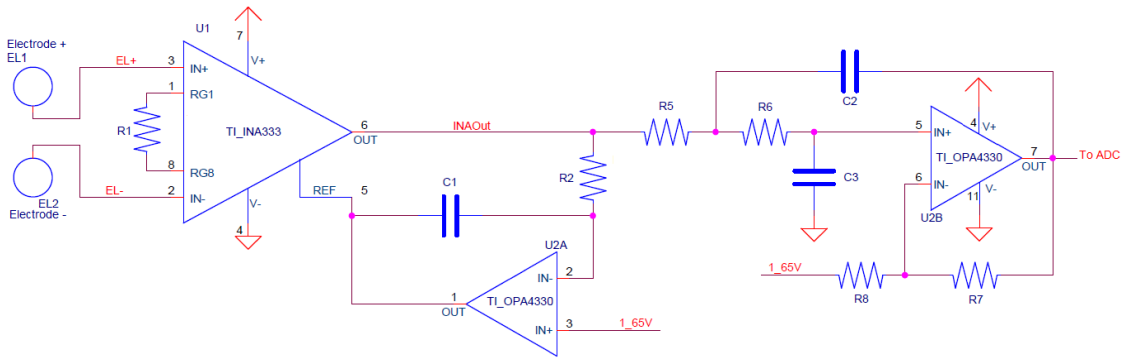

Figure 2.12: Vital ECG analog front-end.

In the first stage, an integrator circuit is used to close the loop between the output of the differential amplifier and its reference voltage. Knowing how a three op-amp differential amplifier -such as the INA333 [40] employed in Vital ECG- works makes it trivial to find that the transfer function is that of a first order high pass:

$$H_1(s) = \mathrm{INA}_{\mathrm{GAIN}} \cdot \frac{sR_2C_1}{1 + sR_2C_1} \tag{2.6}$$

The second stage consist of a well known Sallen-Key cell circuit, which has the following transfer function:

$$H_2(s) = \left(1 + \frac{R_7}{R_8}\right) \cdot \frac{1}{1 + C_3(R_5 + R_6)s + C_2C_3R_5R_6s^2} \tag{2.7}$$

Thus, the combined transfer function with three poles and a zero has the following form:

$$H(s) = H_1(s) \cdot H_2(s) = \mathrm{A} \cdot \frac{sR_2C_1}{1 + sR_2C_1} \cdot \frac{1}{1 + C_3(R_5 + R_6)s + C_2C_3R_5R_6s^2} \tag{2.8}$$

where A is the combined gain of the INA333 and the Sallen-Key cell. The high-pass and low-pass cut-off frequencies has been set at 0.5 Hz and 40 Hz respectively. Being a second order filter, the low-pass side was designed according to the Butterworth function. The total gain was set at 750 where the INA333 accounted for 5 and the Sallen-Key for the remaining 150.

The second stage is directly connected to the micro-controller's 12-bit ADC, which samples the signal at a frequency of $1ksps$ (samples per second).

The power consumption of Vital ECG is a major improvement over ECG Watch. It was measured an average value of $160\mu W$ during stand-by, and $30mW$ during transmission. Estimating a heavy use of 50 acquisition per day, the $120mAh$ battery can last around 40 days.

2.2.2 Performance Evaluations

Despite having many more sensors, most of them were never actually used because of some inner limitations of the CC2640R2F. Therefore only the ECG is taken in account in this section.

Vital ECG was evaluated with the same tests described in the previous section for what regarded ECG Watch. However, the GE B105 was not available, therefore the reference device in this case was a GE MAC2000 [54]. The MAC2000 is a professional electrocardiograph capable of 12-leads recording as well as some advanced heart rhythm recognition features.

The tests involved 36 healthy subjects, evenly distributed between males and females in an age group in the range of $25-35$ years old. For these tests the MAC2000 was configured with four stainless steel clamps electrodes placed on the limbs, and set with a monitor filter. It would have been unfair to compare Vital ECG with an professional electrocardiograph configured in diagnostic mode. Vital ECG, instead, was used to acquire lead I ECGs. The experiment involved 5 simultaneous ECG acquisitions for each patient using both Vital ECG and MAC2000.

Vital ECG data was further filtered with a second order 50 Hz notch filter and a first order low-pass filter set at 40 Hz. Unlike Vital ECG, MAC2000 does not save raw data, therefore no further filtering was applied.

Heart-rate

Figure 2.13 shows the heart-rates estimations Bland-Altman plot for Vital ECG and MAC2000. Despite having a mean value closer to zero, w.r.t the comparison between ECG Watch and B105, the results are more scattered and less consistent. Cross-correlation was evaluated and resulted at 90.5%, which further shows how data is less reliable.

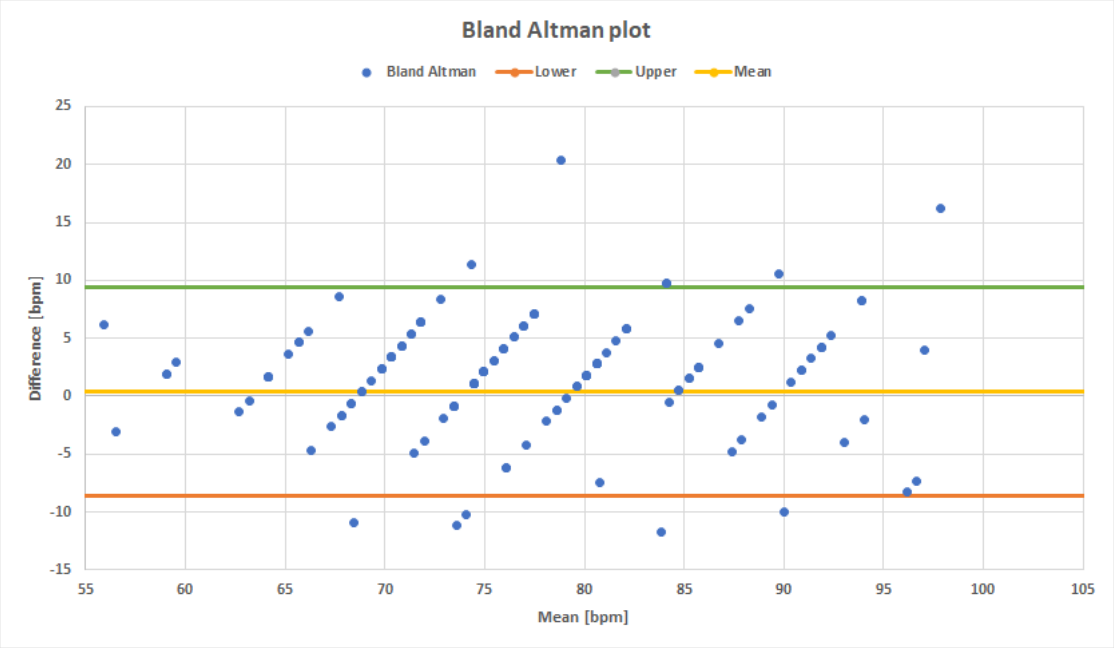

Figure 2.13: Bland-Altman plot of heart-rates estimated from Vital ECG and GE MAC2000 acquisitions.

Power Spectral Density

Figure 2.14 shows the estimated PSD for both Vital ECG and MAC2000 restricted in a band of $[0 - 45]$ Hz. Even just qualitatively it is already evident how, although they have the same underlying shape, Vital ECG has a very different frequency content, which suggests more noise.

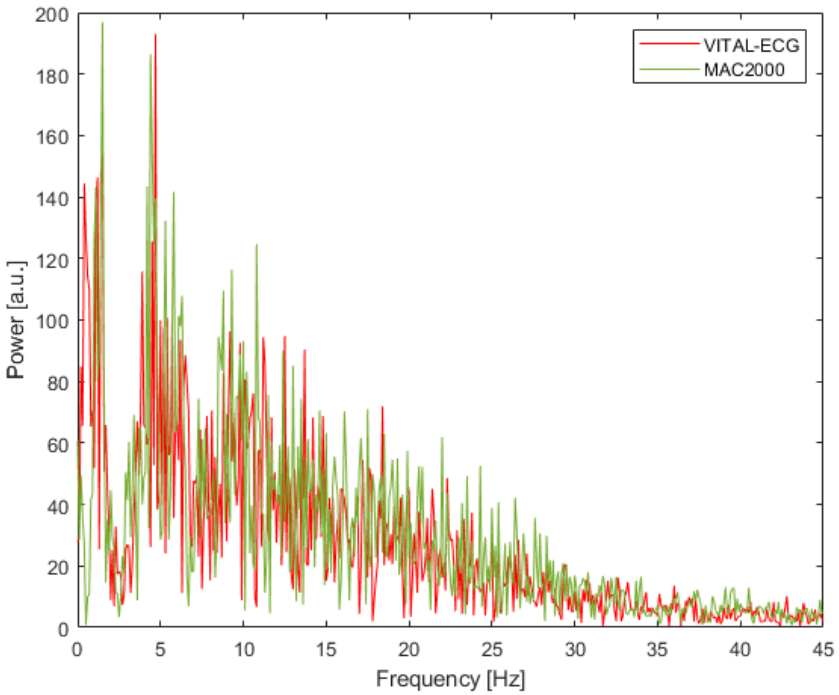

Figure 2.14: PSD plot of Vital ECG and GE MAC2000 signals. The band was restricted to $0 - 45Hz$ in order to highlight differences.

The CSP analysis, resumed in Table 2.4 shows quantitatively what already evinced from Figure 2.14. MAC2000 is capable of recording more information in a wider frequency range, w.r.t the bandwidth of interest.

Table 2.4: CSP Analysis for Vital ECG and GE MAC2000. Frequency of interest.

Device	$f_{20\%}[Hz]$	$f_{50\%}[Hz]$	$f_{80\%}[Hz]$
GE MAC2000	5.5	13.6	31.9
Vital ECG	4.3	11.4	25.6

Signal-to-Noise Ratio

The SNR was defined to follow the same configuration of the ECG Watch and B105 comparison. Therefore the bandwidth of interest is still set at $[0.67 - 40Hz]$. The results resumed in Table 2.5 better prove how Vital ECG cannot compete with MAC2000.

Table 2.5: SNR Analysis for Vital ECG and GE MAC2000.

Device	Mean $[dB]$	Standard Deviation $[dB]$
GE MAC2000	155.8	11
Vital ECG	119.9	12

Time domain differences

The final test involve a direct comparison in the time domain. Figure 2.15 shows the same heartbeat as acquired by Vital ECG and MAC2000. Qualitatively, there is a massive difference between the two signals, as it looks like they are two different heartbeats.

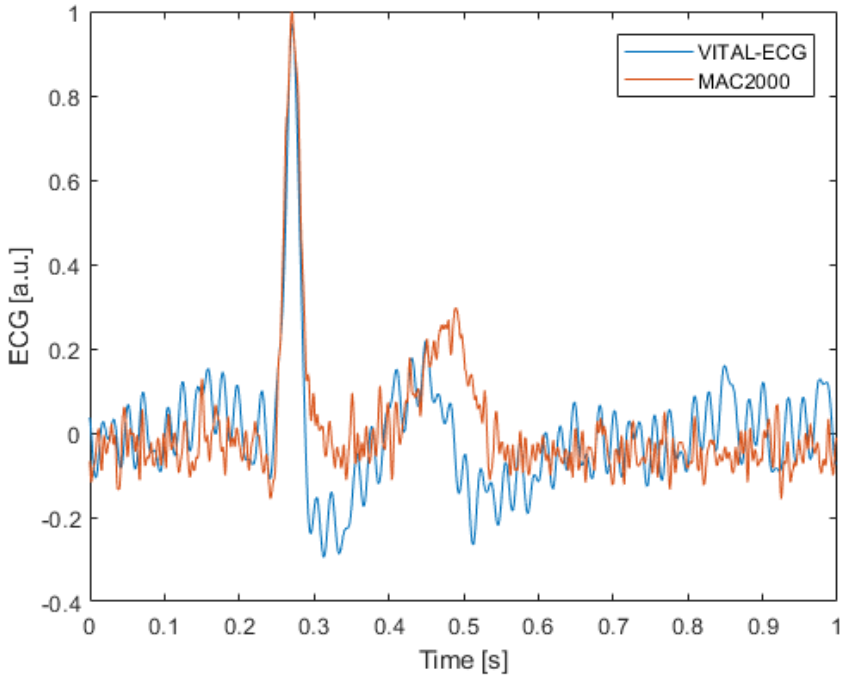

Figure 2.15: The same heartbeat acquired using Vital ECG and GE MAC2000.

However, the results resumed in Table 2.6 are not as exaggerated as the image suggests.

Table 2.6: Time domain difference Analysis for Vital ECG and GE MAC2000.

Mean $[a.u.]$	Standard Deviation $[a.u.]$	Max $[a.u.]$
-0.011	0.1213	0.28

In conclusion, it is undeniable that MAC2000 offers incomparable results w.r.t. Vital ECG, however it is also unfair to compare a bulky and very expensive professional-grade electrocardiograph with a low-cost wearable monitoring-grade one.

2.3 PulsECG

Despite not being able to meet its expectation Vital ECG still provided valuable insight on the problems of wearable devices. However, the issue with Vital ECG was not regarding the quality of its ECG recording, for which it could have been done more in terms of better digital filtering; but rather the fact that its microcontroller was unable to successfully handle the massive amount of data that it was supposed to gather from all its sensors. Moreover, the generous dimensions required to accommodate all components on the PCB still forced to keep an anachronistically thick outer case. These limitations had a huge impact during the outlining of the technical specification of Vital ECG's direct evolution: PulsECG.

PulsECG (Figure 2.16) is currently the latest iteration of wearable ECG devices developed in Neuronica Lab. The main goal of PulsECG was to obtain the most reasonably small device without compromising the ECG quality. Unlike Vital ECG, PulsECG does not include an IMU and a temperature/humidity sensor. Moreover, it uses a satellite board for the pulse oximeter sensor, which can be used synchronously with the ECG circuit. The result is a considerably smaller PCB with a more complex analog front-end.

(a) Front view.

(b) Back view.

(c) Inside.

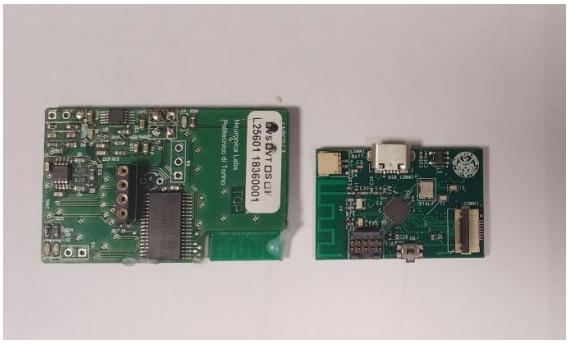

(d) Size comparison with ECG Watch.

Figure 2.16: PulsECG.

2.3.1 Hardware

PulsECG uses the same TI CC2640R2F micro-controller in Vital ECG. Despite having a very similar block diagram (Figure 2.17), the pulse oximeter and the ECG circuit are different.

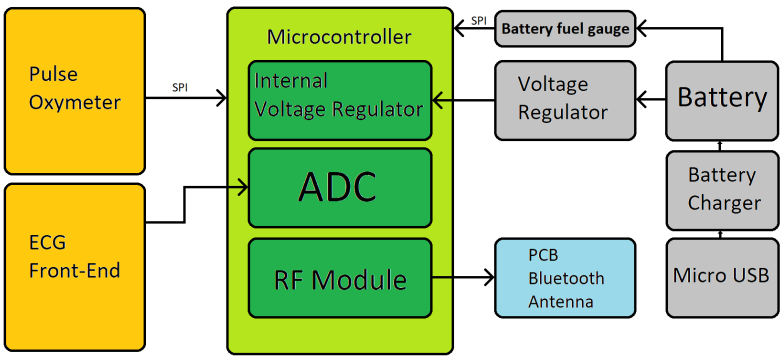

Figure 2.17: PulsECG block diagram.

The new analog front-end (Figure 2.18) is an improved version of the one present in Vital ECG (Figure 2.12). Because of its complexity it can be divided in five

different stages, shown in Figure 2.19.

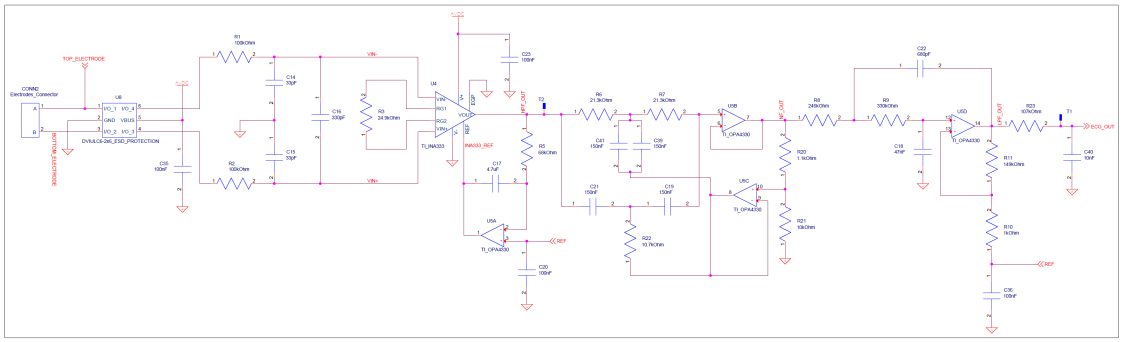

Figure 2.18: PulsECG block diagram.

Starting from the first stage (Figure 2.19a) there is the electrode connector and an Electro-Static Discharge (ESD) protection circuit, which purpose is to save the delicate differential amplifier that is connected to the outer world.

What follows stage one is a pre-filtering stage (Figure 2.19b) in the form of two paired differential and common-mode low-pass filters. The cut-off frequency is respectively of 48 kHz and 4.8 kHz. The common-mode cut frequency has been chosen one decade earlier than the differential one in order to neglect the resulting common-mode component that arise from the inevitable differences between the components used in the filter (even 1% tolerances can create common-mode noise).

The third stage (Figure 2.19c) is completely analogous to the first stage of Vital ECG's front-end (Figure 2.12). Even in this case the high-pass cut frequency is set at 0.5 Hz.

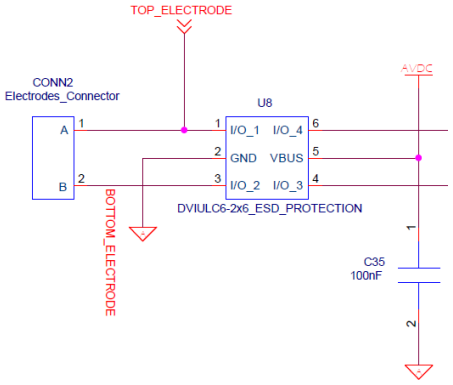

(a) Stage 1.

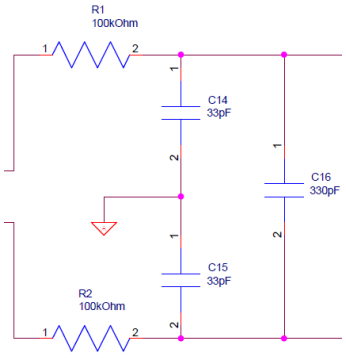

(b) Stage 2.

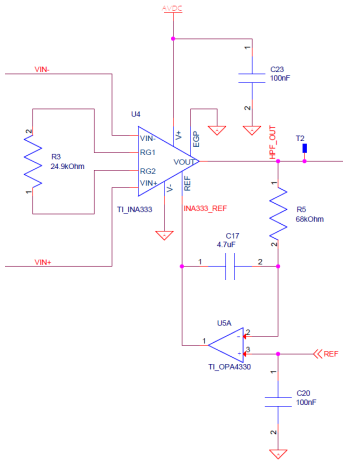

(c) Stage 3.

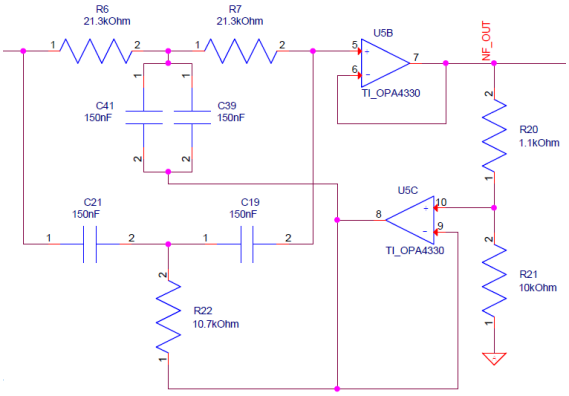

(d) Stage 4.

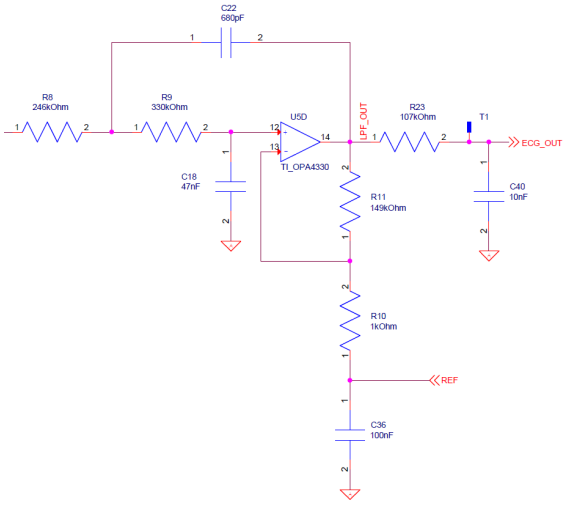

(e) Stage 5.

Figure 2.19: PulsECG analog front-end divided in different stages.

Stage four (Figure 2.19d) contains an active twin-T notch filter [55], for which the transfer function in the Laplace domain (s) is:

$$H_{\text{Twin-T}}(s) = \frac{s^2 + \omega_0^2}{s^2 + \frac{s\omega_0}{Q} + \omega_0^2} = \frac{s^2 + \left(\frac{1}{RC}\right)^2}{s^2 + s\left(\frac{1}{RC}\right)\left(\frac{4}{1+\frac{R_{21}}{R_{20}}}\right) + \left(\frac{1}{RC}\right)^2} \tag{2.9}$$

Where $R = R_6 = R_7 = 2R_{22}$ and $C = C_{19} = C_{21} = C_{39} = C_{41}$. In this design the notch frequency $f_0 = \omega_0/(2\pi)$ was set at 50 Hz, while the quality factor $Q = (1 + R_{21}/R_{20})/4$ was set to 2.523.

Finally, the fifth stage (Figure 2.19e), is similar to the second stage of Vital ECG's front-end. However in this case the cut-off frequency is set at 100 Hz, designed using the Bessel function.

The analog front-end's output is fed into the micro-controller's 12-bit ADC, and the signal is sampled at a sampling frequency of 500 samples per seconds (sps), which is half of what used for ECG Watch and Vital ECG. Lowering the sampling frequency was an acceptable trade-off in order to be able to transfer ECG and PPG (photoplethysmogram) data in real time. Having set the low-pass cut-frequency at 100 Hz, the minimum sampling frequency required to avoid aliasing (according to Nyquist-Shannon theorem) is 200 *sps*, which is considerably lower than 500.

Despite the presence of multiple physical filters, PulsECG still provides a rather raw and pure signal that has to be further processed once the acquisition is over. Because of RAM memory limitations, post-processing is not handled directly in the micro-controller, but rather on the app, which still provides a way to save the raw signal in case it is needed. During the post-processing the signal passes through different passages. First, the signal's average value is removed from every sample, to center it around the zero. Then an Infinite Impulse Response (IIR) filter, implementing a 10^{th} order comb, is applied; followed by a moving average filter with window length set to 10 samples. The results are showed in Figure 2.20.

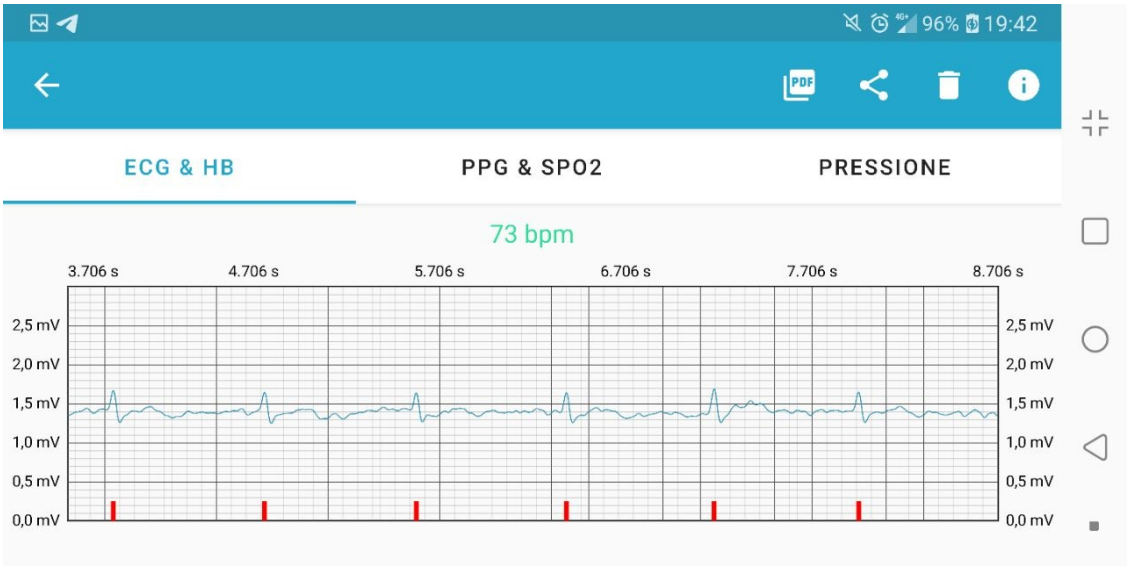

Figure 2.20: ECG signal acquired using PulsECG, as seen from the Android application.

For what it regards the pulse oximeter, PulsECG incorporates the newer Maxim MAXM86161 [56]. With regards to its predecessor (MAX30102), this sensor has: a significantly improved ambient-light cancellation, a better ADC, lower power consumption, smaller dimension, and some useful software functionalities. Amongst the latter, there is an interrupt pin that can be associated to an internal proximity sensor, besides other functions. This proximity sensor has been exploited as a trigger for the whole acquisition, acting as a starting signal for the system so that users can begin an acquisition at their own pace. Figure 2.21 shows the PPG signal acquired by PulsECG. Note that the results shown in Figure 2.20 and Figure 2.21 are acquired synchronously during the same acquisition.

Figure 2.21: PPG signal acquired using PulsECG, as seen from the Android application.

2.3.2 Performance Evaluations

Because of the Coronavirus disease 2019 (COVID-19) pandemic, it was impossible to launch an acquisition campaign for a formal evaluation of PulsECG. Qualitatively speaking the results are more in line with the performance of ECG Watch, albeit more defined, than those of Vital ECG.

Chapter 3

Arrhythmia pattern recognition

In the previous chapters it was illustrated how the inclusion of ECG capabilities in portable or wearable devices have a huge potential in terms of preventing or monitoring cardiovascular conditions. However, as ECG capable devices become more and more common there is still an open problem on how to handle the massive amount of data they produce. Regardless of how detailed and clear an ECG appears, it is nothing but a scribble on a paper sheet without proper interpretation. Interpretation, however, comes at the cost of having an expert analyzing the recording, which is not cheap neither in terms of money, nor time. Furthermore, it would be completely unreasonable to deliver each and every acquisitions, even those that might be clearly flawed, to be analyzed as it would require a inhumane effort just to keep up with as the user base grow. However, there are two key concepts here that could be exploited: the first is that cardiologists, being restricted by human limitations, can only analyze a handful of ECG per day; the second is that a cardiologist only needs to analyze an ECG showing some sort of anomaly in order to actually make a diagnosis, all other rhythm that does not exhibit any strange behavior could be ignored. Starting from these two assumptions, the only logical solution is that an algorithm that filters out normal rhythms, while highlighting abnormal ones could be used. In this way only the few ECGs that exhibits anomalies are sent and analyzed by doctors, while all the others can be ignored. In addition, it would greatly help the ECG evaluation if the algorithm could also further highlight the anomaly it found in terms of associating it with an arrhythmia, in order to triage it. Because some rhythm alterations are more dangerous than others, and therefore require a prompt and accurate analysis even if it is just a false positive. For instance: an ECG that shows an elevation of the ST segment can be associated with acute myocardial infarction [57] and thus should have maximum priority so that, if it is confirmed, an ambulance can be dispatched as soon as possible.

Automatic rhythm recognition in ECG application is not a novel problem. In fact, the first documented attempt of an automated analysis dates back in 1960, with a description of a *automatic processing of electrocardiograms leading to their*

analysis by digital computer [58]. However, despite the colossal improvement of technology and techniques, automatic rhythm recognition is still today an open problem. During the years there have been, of course, various valuable contributions on the matter, such as [59, 60, 61, 62]. Nonetheless, most of the proposed algorithm -if not all of them- focus the attention on a single arrhythmia, in the attempt of simplifying the problem, which is a widely used paradigm in computer science also known as *divide-et-impera*. The result is that there is still the lack of a reliable algorithm capable of interpreting an ECG and formulating a generic diagnosis with a reasonable degree of accuracy. The reason behind this is that heartbeat recognition is an intrinsically difficult task. It is hard to generalize rules that can be easily programmed to a computer because even for humans there is not a definite rule set, but rather an interpretation method, which requires practice and experience. In an attempt to mimic the human approach, data-driven programming is a paradigm of computer science in which algorithms derive their operation from a data-set, rather than a defined sequence of steps. In a certain sense, these algorithms can learn from data and extrapolate an interpretation. For this reason data-driven programming can be considered the paradigm that gave birth to machine learning.

In recent years machine learning gained a lot of momentum due to the great success that it had on consumer-level application such as: the natural language processing involved in common virtual assistants like Siri [63] or Cortana [64]; or the image segmentation and classification used in face recognition software [65]; or the mixed sensor analysis used in self-driving car; etc. Obviously this success also translated into adopting the various technologies involved machine learning also for health related applications. For instance: deep learning models are widely used for medical image processing in improving images, spotting anomalies, dividing images in zones, extrapolating data, etc. A notorious case is IBM Watson, which was both praised and criticized [66] for being able to detect, in some cases, skin cancers from images better than humans [67]. A final, more recent, example is a neural model that was employed to design drugs became infamous for being exploited to find toxins, and being able to discover over 40000 of them in less than 6 hours [68, 69].

There are a numerous applications of machine learning for ECG pattern recognition in literature. A few examples include: [70, 71, 72, 73]. However, as none of them succeeded in developing a reliable generalized arrhythmia recognition model, the problem of finding one is still open.

A novel approach to the ECG pattern recognition problem is proposed in this chapter, involving the use of mono-dimensional Convolutional Neural Networks (1D-CNN).

3.1 Mono-dimensional Convolutional Neural Networks

Convolutional Neural Networks (CNN) are currently a very popular class of neural networks in which a filter -usually called kernel- is passed along the data to learn underlying patterns. 1D-CNNs are a sub-class of CNNs that only deals with mono-dimensional data such as the ECG. This distinction is necessary because CNN are usually employed on images and thus two-dimensional data.

The working principle of 1D-CNNs is presented in Figure 3.1. In this example, a kernel with $k = 3$ elements is convoluted along an input vector of $n = 10$ elements in order to produce a filtered output of $m = n-k+1 = 8$ elements. The convolution process involves a few simple passages: first, the kernel is superimposed to the first k elements of the input vector; then, corresponding elements of the two vectors are multiplied together to form a new element of the output vector; after that the kernel is moved of one (or more) elements with regards to the input vector and the process is repeated until the kernel covers all the input elements.

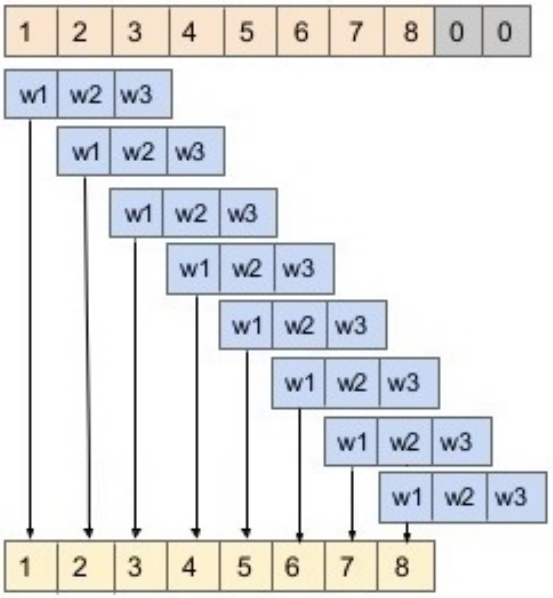

Figure 3.1: 1D-CNN working principle using zero padding.

Because of how a 1D-CNN works the output is necessarily smaller than the input. This effect of data erosion can be a serious problem when applying multiple layers of convolution one over the other. Therefore, it is possible to just add dummy data on both extremities of the input vector in order to compensate the data loss. This expedient is better known as padding, or zero padding when the dummy data consists of zeroes (as shown for example in Figure 3.1).

The whole process is equivalent to filtering the input vector using the kernel in order to extract or highlight specific patterns. Applying multiple layers of 1D-CNN results in a growth of complexity of the extracted patterns. Therefore using enough layers it is possible to use the model to represent patterns with arbitrary complexity. For instance it could be possible to obtain the model of an heartbeat as seen in ECGs.

3.2 Deep network for generalized ECG pattern recognition

A neural network that use of many CNN layers, amongst other layers, is usually referred to as deep neural network.

In this section various deep network architectures are evaluated in order to obtain a model capable of generalized ECG pattern recognition [74]. Namely, a network capable of classifying each and every heartbeat of a ECG signal in order to formulate a diagnosis based on the rhythm.

3.2.1 Dataset

When dealing with CNNs, or any other supervised learning model, the most delicate and difficult part is inarguably the preparation of a dataset. In the context of ECG, the most notorious and reliable source of publicly available data is Physionet [75], which is a repository containing dozens of databases used worldwide for research purposes. From Physionet the MIT-BIH Arrhythmia Database [76] has been selected because of its richness in both terms of different arrhythmias represented, and number of recordings.

The MIT-BIH Arrhythmia Database contains data from 47 different patients presented as two lead ambulatory ECG recordings of 30 minutes length each. What makes this particular database so appealing for supervised learning approaches is that every single heartbeat (approximately 110000 total) has been labelled independently by two cardiologist. In total there are 15 different classification for each heartbeat, plus a jolly class for unrecognizable ones. Table 3.1 resumes the different heartbeat classes and their related label in the annotation file.

The total database consists of over 31 million samples digitalized with a sampling frequency of 360 sps. Therefore, the first step in the dataset preparation is dividing the database in segments small enough to be fed to the neural network, but still large enough to contain at least one heartbeat. For the sake of simplicity a segment size of 500 was chosen, ensuring the presence of at least one heartbeat even in case of bradycardia down to 43.2 bpm. Data augmentation was applied in terms of a 10% overlapping factor between adjacent segments, in order to produce more data for the network training.

Table 3.1: MIT-BIH heartbeat label meaning

Label	Meaning
/	Paced beat
A	Atrial premature beat
E	Ventricular escape beat
F	Fusion of ventricular and normal beat
J	Nodal premature beat
L	Left bundle branch block beat
N	Normal beat
Q	Unclassifiable beat

Label	Meaning
R	Right bundle branch block beat
S	Supra-ventricular premature beat
V	Premature ventricular contraction
!	Ventricular flutter wave
a	Aberrated atrial premature beat
e	Atrial escape beat
f	Fusion of paced and normal beat
j	Nodal escape beat

Once the database was divided in smaller segments, data was normalized in a range of $[-1, +1]$, and the related label was assigned to the segment.

The final dataset was produced by randomly dividing the above obtained segments in a training dataset and a validation dataset with a ratio of 90% and 10% respectively.

3.2.2 Experiments

Several network configuration were evaluated to asses the classification quality of a 1D-CNN on the MIT-BIH dataset in search for the best performances in terms of accuracy. During the tests different networks were assembled by varying: number of 1D-CNN layers, 1D-CNN kernel size and, drop-out rate, and the activation function. The most representative and successful are reported in Table 3.2.

Table 3.2: Classification accuracy for the best 1-D CNN architectures

	Training Accuracy	Test Accuracy	Total Parameters
Net 1	92 %	91 %	65,056
Net 2	96 %	94 %	257,104
Net 3	96 %	94 %	533,072
Net 4	98 %	95 %	1,266,768

The simplest of the proposed networks, *Net 1*, achieved an accuracy equal to 92% and 91% respectively during training and validation. *Net 1*, which counted around $65K$ parameters, consisted of a single convolutional layer containing 16 filters with kernel size 32; followed by a max pooling layer, that compress the output information in a smaller vector easier to elaborate; a drop-out layer, required to reduce over-fitting; a flatten layer, which reorders the output array in a vector; a

fully dense layer, that further elaborates the output; and finally a softmax classifier required for the output of the system.

The second network proposed, *Net 2*, composed of roughly $257K$ parameters consisted of a convolutional layer with 64 filters of size 8, followed by the same layers found at the end of *Net 1*. *Net 2* was able to achieve an accuracy value of 96% during training, and 94% during validation, improving the results obtained with *Net 1*.

Net 3 is the first one using a deep approach. It is composed of three convolutional layers with growing number of filters and decreasing kernel size, each interleaved by max pooling layers. The following layers of the network are analogous to those in the tail of *Net 1* and *Net 2*. The first convolutional layer of *Net 3* has 64 filters of 32 elements, while the second has 128 filters sized 16 elements, and the third has 256 filters with size 8. Despite doubling the parameter numbers there was no difference in terms of accuracy between *Net 2* and *Net 3*, sign that the model had encountered a plateau of performances.

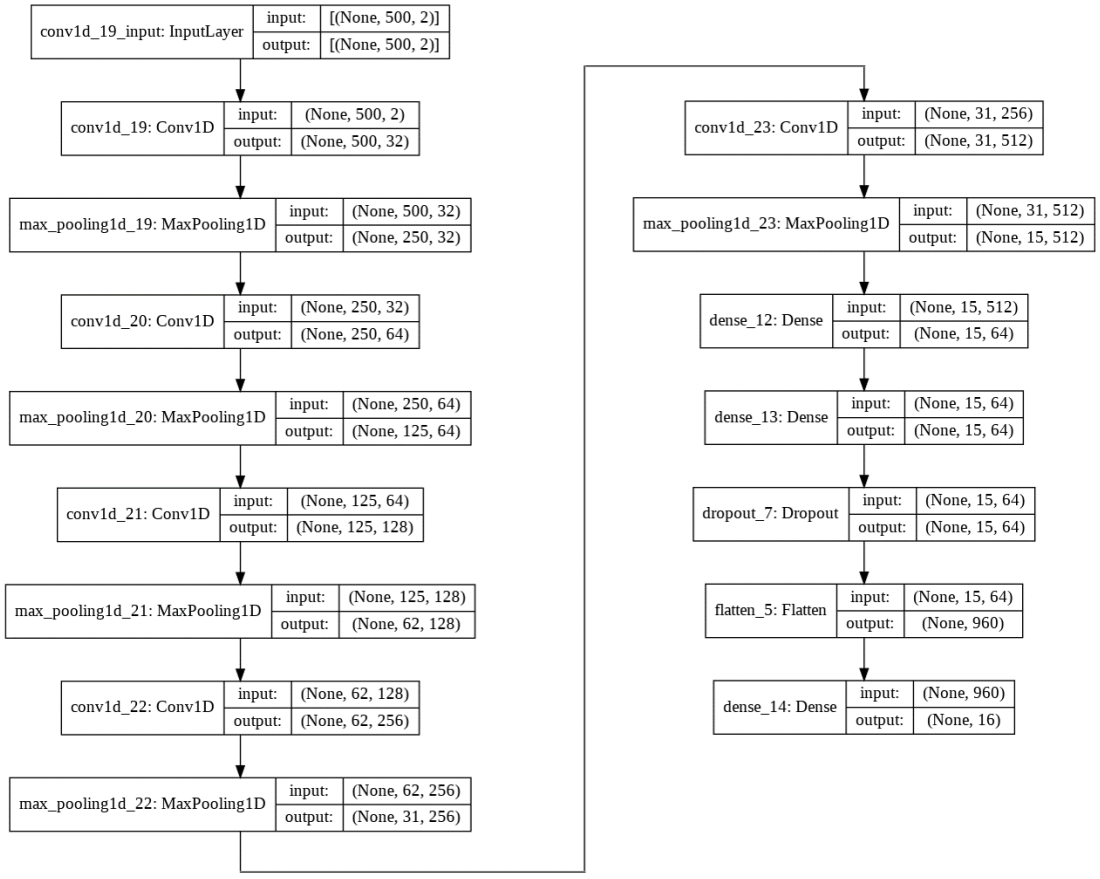

Figure 3.2: *Net 4* architecture.

The final and deepest network proposed is *Net 4*, with its $1.2M$ parameters. This network, represented schematically in Figure 3.2, has a grand total of five convolutional layers. The filter parameters followed the same approach of *Net 3* doubling the number of filters while halving the sizes in each consequent layer. Therefore first of those has 32 filters of 128 elements, while the fifth has 512 filters of size 8. *Net 4* achieved an accuracy score of 98% and 95% in training and validation respectively.

3.2.3 Results

Despite *Net 4* was followed by several networks with much higher parameters count, it was impossible to find a better model. It was only after the analysis of *Net 4* confusion matrix (Figure 3.3) that it was clear why all further attempts failed.

A confusion matrix is a table used to highlight the performance of a classification algorithm in a visual form. In a confusion matrix columns represent the expected value, while rows represent predicted ones. Cross evaluating the predicted value with the expected one gives information on the accuracy for each class. Therefore, the confusion matrix of a perfect classifier is an identity matrix.

There are a few considerations to be made by observing Figure 3.3. The first one is that class F, which represents the fusion of ventricular and normal beat, is often confused with the class N, which represents normal beats; and class V, which represents premature ventricular contractions. However, depending on how the input segment was obtained a class F beat can result indistinguishable from a class N or a class V. A solution to improve F classification could be to enlarge the segment size, at the cost of lowering the classification of other heartbeats.

Class S, which represents supra-ventricular premature beats; was completely misinterpreted as class V, which instead represents premature ventricular contractions. This is due to the fact that these two beats are very similar when examined in lead I and lead II, which were the only available ECG signals for the network.

Class e, which represents atrial escape beats, is recognized as a different class in 94% of the cases. After a deep investigation it was found a that the class e was severely underrepresented in the input dataset, consisting of just 2% of the total segments.

Finally, because of its nature it is not surprising that class Q is recognized as many different classes. In fact, class Q represents unclassifiable heartbeats. Namely, those heartbeats that the two cardiologists that examined and commented the signals were not able to classify due to noise, uncertainties, alterations, etc. Therefore, albeit the net classified erroneously those hearbeats, it is not possible to exclude without further investigation that the network was actually responding to some specific pattern learned from the correct class.

In conclusion, the confusion matrix analysis highlighted the fact that a data-driven model can only be as good as the data used to synthesize it. If the data does

not represent the problem, then it is impossible to find a proper solution. With a better dataset it could be possible to find a model capable of representing all 16 classes with an accuracy higher than 96%. However, with the data at disposal this is the best that this network could achieve.

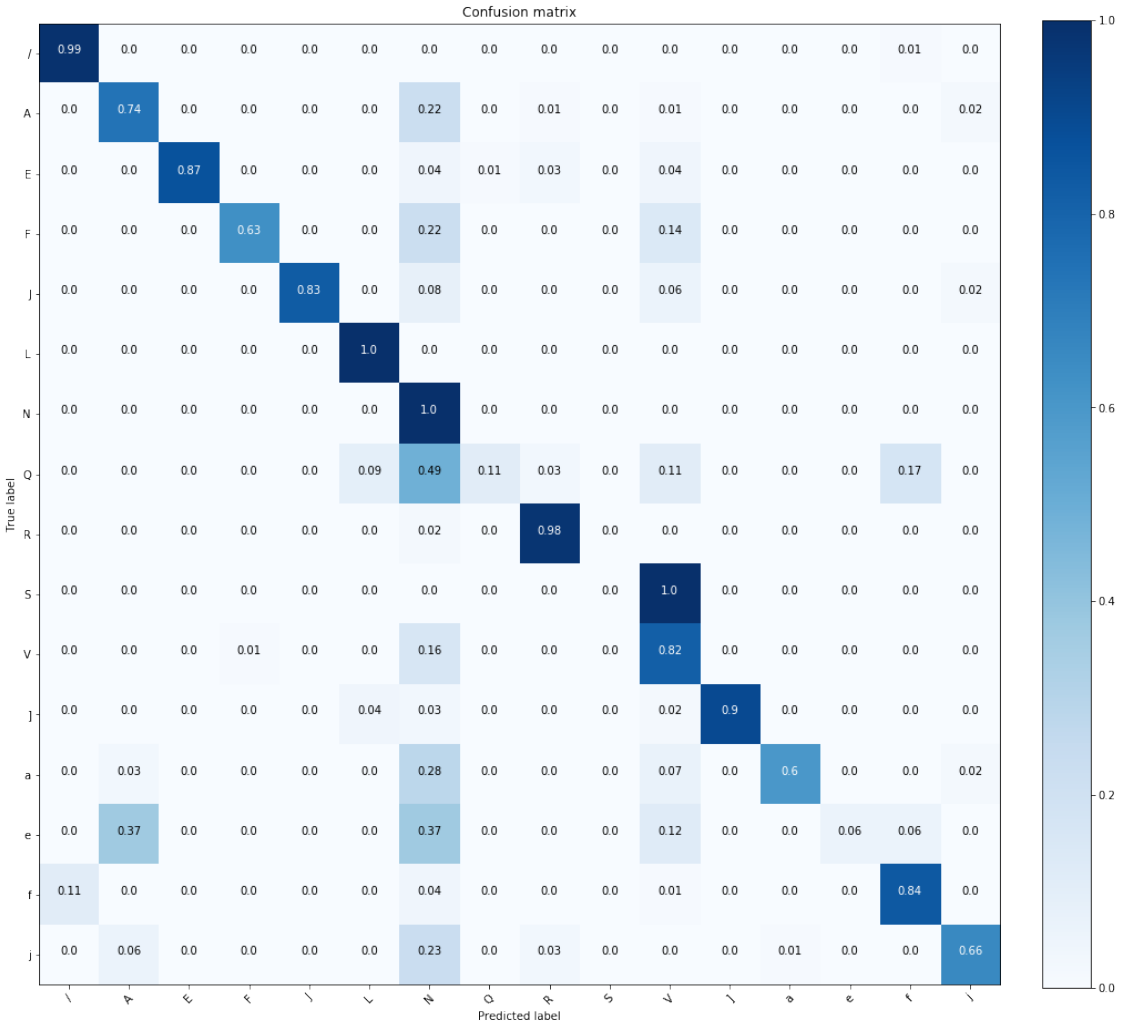

Figure 3.3: *Net 4* confusion matrix.

3.2.4 Comparison with other networks

Despite the result being far from perfection, *Net 5* obtained comparable results with other network using a less generalized approach. In fact, there are in literature many networks designed for ECG pattern recognition, but they usually aim to simplify the problem by reducing the number of patterns to recognize. For example in [77] a very deep network with thirteen convolutional layers is used to classify five of the sixteen available rhythms in the MIT-BIH dataset with an overall accuracy

of 93.4%. In [78], the different rhythms are divided in five macro-classes according to the AAMI EC57 [79] standards. The network proposed in this case consists of three convolutional layers capable of achieving an accuracy of 92.7%. A similar approach was used in [80] achieving an accuracy of 97.3

A completely different approach was used in [81] and [72] where the ECG signal is treated as a 2D image and analyzed with massive networks achieving respectively an accuracy of 98% and 80% in recognizing 6 and 12 different arrhythmia respectively. Albeit none of the presented studies used all 16 available classes, it is evident how growing in complexity causes a degradation of the performances.

Finally, in [82] Generative Adversarial Networks (GANs) are used to produce data in order to re-balance the MIT-BIH dataset and, thus, represent all classes equally. Consequentially, the classifying network, inspired by the inception network [83], achieved an accuracy of 98% when used to recognize 15 different patterns, proving that a generalized approach is possible when the initial dataset is balanced. In this case, however, the network consists of different million parameters, which could easily lead to over-fitting problems when exposed to a more robust dataset.

3.3 1D-CNN for non-generalized ECG pattern recognition

The final observation made for the generalized model suggested that it could be possible to re-balance the input dataset in order to achieve better performances. To this purpose, a different non-generalized model is proposed, named $Net5$, aimed at classifying not all the available classes, but just the four more represented: N, V, R, and A. The remaining classes, some of which were under-represented, and others had intrinsic problems in their recognition, are instead grouped in a new super-class O, namely *others*.

In this case a simpler net with just 4053 parameters was enough to achieve a training accuracy over 99.9% and a validation accuracy around 99.6%. *Net 5*, which is shown in Figure 3.4, has four convolutional layers with the following composition: the first one has 4 filters of size 4, the second one has 6 filters of size 6, the third contain 8 filters with 10 elements, and the forth and final consist of 10 filters with 16 elements.

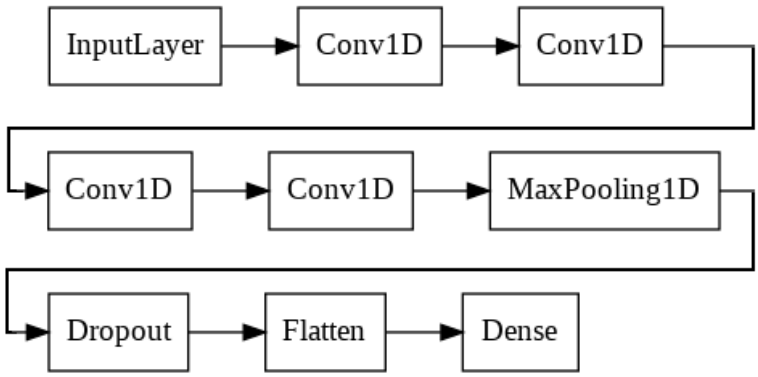

Figure 3.4: *Net 5* architecture.

Figure 3.5 shows the confusion matrix, which is almost an identity.

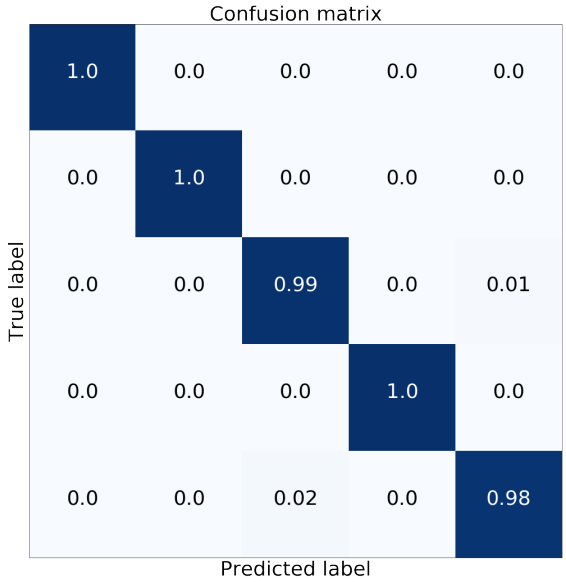

Figure 3.5: *Net 5* confusion matrix.

3.4 Feature extraction in ECG classification: a comparison between 1D-CNN and feature engineering

Neural networks, and in particular deep convolutional networks, are usually referred and treated as black boxes. Although the accuracy and efficiency of CNN-based approaches is undeniable, their ability in extracting and using features extracted from raw signals is still barely understood. In other words: the combined complexity and abstraction of a CNN makes almost impossible to understand and explain in human terms how the network is achieving its results. For this reason, the previous discussed networks were employed in another research in an attempt to uncover differences and relationships between CNN feature maps and human-curated temporal features, towards a deeper understanding of neural-based approaches for ECG classification [84].

In contrast to CNN, feature engineering relies on domain experts, e.g. cardiologists, to extract relevant information from data. The extracted feature can then be analyzed with statistical means, or by using non-deep neural networks, which are intrinsically easier to explain than CNN. With regards to [85] fifteen temporal features, resumed in Table 3.3, are extracted and used to train a Multi-Layer Perceptron (MLP) which was consequently used for ECG classification.

The main goal of this study is not to obtain the best ECG classification model, but rather to assert whether deep networks are capable of extracting similar features with regards to feature engineering. This would provide a valuable insight of how a deep CNN handles data towards its layers as well as confirming the validity of the extracted features in ECG classification models.

3.4.1 Cross-Correlation analysis

Given a pair of random variables X and Y coupled with their respective probability density function f_X and f_Y; the probability density function of their difference f_{X-Y} is known as *cross-correlation*.

$$f_{X-Y} = f_X \star f_Y \tag{3.1}$$

The cross-correlation can be seen as a measure of similarity between the two starting random variables X and Y. When, instead, it is applied to two random vectors $\mathbf{X} = (X_1, \ldots, X_m)^T$ and $\mathbf{Y} = (Y_1, \ldots, Y_n)^T$, the resulting cross-correlation matrix has the form given by:

$$R_{\mathbf{XY}} := \mathbb{E}[\mathbf{X}\mathbf{Y}^T] \tag{3.2}$$

However, in order to simplify interpretation the cross-correlation matrix can be normalized and expressed as:

Table 3.3: Temporal features extracted from the ECG raw data.

#	Attribute	
F1	Mean	$\bar{x} = \sum \frac{x_i}{N}$
F2	Max value	$max\,(x)$
F3	Root Mean Square (RMS)	$\sqrt{\sum \frac{x_i^2}{N}}$
F4	Square Mean Root (SMR)	$\left(\sum \frac{\sqrt{\lvert x_i \rvert}}{N}\right)^2$
F5	Standard deviation	$\sqrt{\frac{1}{N-1}\sum (x_i - \bar{x})^2}$
F6	Variance	$F5^2$
F7	Shape factor (using RMS)	$\frac{F3}{\sum \frac{\lvert x_i \rvert}{N}}$
F8	Shape factor (using SMR)	$\frac{F4}{\sum \frac{\lvert x_i \rvert}{N}}$
F9	Crest factor	$\frac{F2}{F3}$
F10	Latitude factor	$\frac{F2}{F4}$
F11	Impulse factor	$\frac{F3}{\sum \frac{\lvert x_i \rvert}{N}}$
F12	Skewness	$\frac{\frac{1}{N}\sum (x_i - \bar{x})^3}{\left[\frac{1}{N-1}\sum (x_i - \bar{x})^2\right]^{\frac{3}{2}}}$
F13	Kurtosis	$\frac{\frac{1}{N}\sum (x_i - \bar{x})^4}{\left[\frac{1}{N-1}\sum (x_i - \bar{x})^2\right]^{2}}$
F14	Normalized 5th central moment	$\frac{\frac{1}{N}\sum (x_i - \bar{x})^5}{\left[\frac{1}{N-1}\sum (x_i - \bar{x})^2\right]^{\frac{5}{2}}}$
F15	Normalized 6th central moment	$\frac{\frac{1}{N}\sum (x_i - \bar{x})^6}{\left[\frac{1}{N-1}\sum (x_i - \bar{x})^2\right]^{3}}$

Where: N is the number of elements of the input vector x, while x_i is the i^{th} element.

$$\rho_{\mathbf{XY}} = \frac{\mathrm{cov}(\mathbf{X}, \mathbf{Y})}{\sigma_{\mathbf{X}} \sigma_{\mathbf{Y}}} \tag{3.3}$$

which is in the range $[-1, +1]$, with 1 indicating a perfect correlation, -1 a perfect anti-correlation, and 0 no correlation at all.

The normalized cross-correlation (Equation 3.3) has been employed as similarity measure to assert whether the engineered feature of Table 3.3 are present in any of the feature map generated by the 1D-CNN. Therefore, for each sample (i), each filter (j), and each extracted feature (k); the normalized cross-correlation was computed to evaluate similarities between the 1D-CNN feature map $x_i^j = (x_{i1}^j, \ldots, x_{im}^j)^T$

and the temporal representation of the sample $x_i^k = (x_{i1}^k, \ldots, x_{in}^k)^T$:

$$\rho_{x_i^j x_i^k} = \frac{\text{cov}(x_i^j, x_i^k)}{\sigma_{x_i^j} \sigma_{x_i^k}} \tag{3.4}$$

Averaging this score across all samples for each convolution filter it is possible to evaluate the average similarity between feature maps and the extracted features:

$$\rho_{j,k} = \frac{1}{N} \sum_{i}^{N} \rho_{x_i^j x_i^k} \tag{3.5}$$

Similarly to Equation 3.3, this score ranges in $[-1, +1]$ with the same interpretation. Equation 3.5 is the final score that was used to investigate the abstraction level of the extracted features with regards to the feature maps extracted by the 1D-CNN.

Because of the implication of this study, a very deep net (Figure 3.6) with similar results of *Net 4* was employed. This network contains ten convolutional layers with progressively higher number of filters and kernel dimension. The first convolutional layer employes 4 filters with 8 elements, the second and the subsequent layers doubles the number of filters or their dimension alternatively until the last layer with 128 filters of size 128. The main idea behind this peculiar architecture is that the first layers are supposed to extract less complicated temporal features, while descending deeper in the network the extracted features' complexity grows exponentially, providing more abstract characteristics.

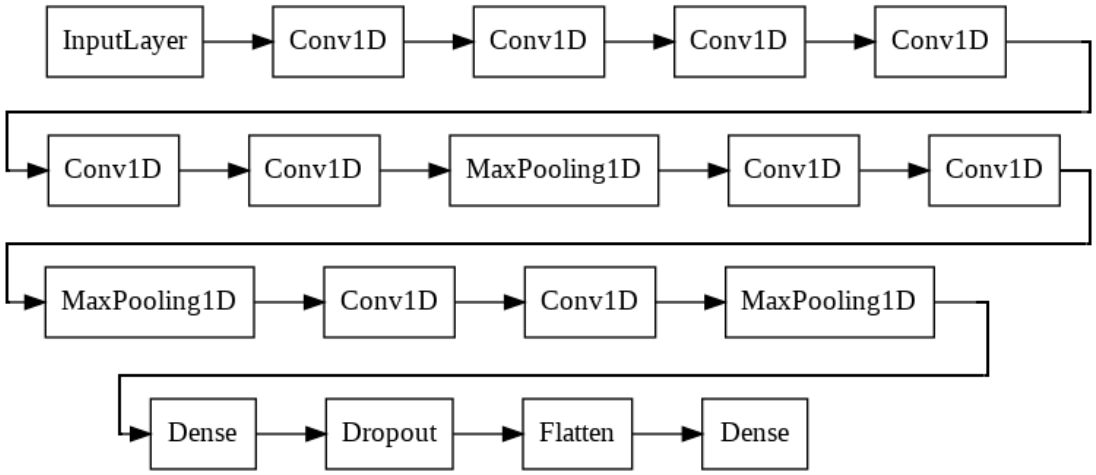

Figure 3.6: *Net 6* architecture.

The extracted features are compared with the 1D-CNN feature maps by mean of (3.5) in order to assert *if* and *how* the network is capable of extracting temporal

features from ECG signals. The results are resumed in Table 3.4 where: for every feature the minimum and the maximum normalized cross-correlation has been reported with its corresponding feature map and filter.

Table 3.4: Maximum and minimum $\rho_{j,k}$ between temporal features and CNN feature maps. The highest and lowest similarity values are highlighted in bold.

Temporal feature		Layer	Filter	ρ
F1	MAX	1	2	0.497
	MIN	**1**	**1**	**-0.882**
F2	MAX	1	2	0.685
	MIN	**1**	**1**	**-0.808**
F3	**MAX**	**1**	**2**	**0.875**
	MIN	3	7	-0.236
F4	**MAX**	**1**	**2**	**0.882**
	MIN	6	4	-0.252
F5	MAX	1	2	0.748
	MIN	3	7	-0.236
F6	MAX	1	2	0.699
	MIN	3	7	-0.246
F7	MAX	1	2	0.553
	MIN	7	3	-0.180
F8	MAX	2	6	0.658
	MIN	7	6	-0.138
F9	MAX	1	2	0.725
	MIN	**1**	**1**	**-0.838**
F10	MAX	1	2	0.701
	MIN	1	1	-0.700
F11	MAX	1	2	0.711
	MIN	1	1	-0.780
F12	MAX	1	2	0.500
	MIN	1	1	-0.553
F13	MAX	1	4	0.655
	MIN	2	3	-0.048
F14	MAX	2	8	0.532
	MIN	1	1	-0.300
F15	MAX	1	4	0.681
	MIN	3	3	-0.014

From Table 3.4 it is possible to observe how, indeed, the 1D-CNN is capable of extracting temporal-like features which are very similar to those human-engineered. Furthermore, the extracted features are more common in the first layers of the network, indicating that the more abstract features obtained in deeper layers derive from the improvement on those temporal features.

In particular F1, F2, and F9 are strongly anti-correlated with the feature map

generated from the first filter of the first layer; suggesting a response of how steep the peaks are compared to the average. On the other hand, F3 and F4 are strongly correlated to the second filter of the first layer which can be interpreted as the peak-to-peak amplitude.

3.4.2 Classification comparison

As a final investigation on the effective contribution of the features automatically extracted by 1D-CNNs to the ECG classification problem [84], it was conducted a comparison between *Net 5* (presented in section 3.3) and the MLP used in [85]. This MLP consist of a single hidden layer with forty neurons and five output units using the softmax activation function. Comparing the confusion matrixes of *Net 5* (Figure 3.5) and the MLP (Figure 3.7) it is evident how the 1D-CNN is capable of a better classification. These results not only prove that the manually engineered features are effectively useful in ECG classification tasks, but also that deep networks can extract and improve those features by further elaborating them towards higher level of abstraction.

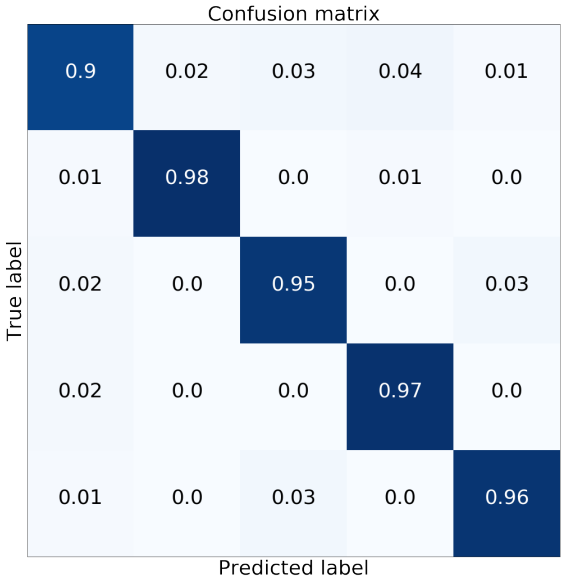

Figure 3.7: MLP confusion matrix.

Chapter 4

Shockable rhythm recognition in Automated External Defibrillators

Automated External Defibrillators (AED) are a peculiar class of defibrillators that require little to none knowledge for their operation. In fact, AEDs are designed to automate most of the decision-making and to guide the operator through all the steps required to resuscitate a Sudden Cardiac Arrest (SCA) victim. Such devices are a life-saving asset that should be readily available in any crowded area such as: train stations, malls, theaters, casinos, stadiums, etc; or any facility with a relatively high risk fo SCA incidence such as gyms, playing fields, nursing homes, etc. It is in fact proven that early defibrillation of SCA can improve the survival rate by over 50%, which is one of the reason why AEDs are referred to as the "single greatest advance in the treatment of VF cardiac arrest since the development of CPR". Most AEDs nowadays also include audio-visual instructions on how to perform Cardio-Pulmonary Resuscitation (CPR), which is the single most important operation to perform on a SCA victim. Furthermore, some of them are also capable of sensing chest compressions in order to give a feedback on the rescuer's CPR performance in terms of depth and frequency [86, 87]. Although some countries require a training by law, their operation is usually simple enough to be used even without any prior knowledge.

To achieve such degree of automation, the most critical aspect of an AED is probably that the device has to formulate an accurate diagnosis on the patient's ECG. The results of misinterpretation are in fact almost always disastrous. In the best case scenario the AED will fail in the recognition of a shockable rhythm, which will result in not delivering the electric shock, and thus losing a chance of stopping the malicious arrhythmia as well as wasting precious time that could make the difference between life and death. On the other hand, if the AED misdiagnoses a non-shockable rhythm as shockable the subsequent delivery of a defibrillation shock to the patient will likely cause Sudden Cardiac Arrest [1]. Thereafter, the AED will be the triggering cause of the very same condition that it was originally designed to

cure endangering the life of a healthy person. Although, for obvious reasons, both kind of misinterpretation are to avoid, the latter has a more dangerous effect, and thus, when in doubt the preferred course of action is to not deliver the shock.

In the previous chapter a novel approach on ECG classification employing mono-dimensional Convolutional Neural Networks (1D-CNN) was presented [74, 84]. However, despite the good results that such networks could achieve in discriminating shockable from non-shockable rhythms, 1D-CNNs are inherently hard to compute. Even *Net 5*, which the smaller network proposed, has over 4000 parameters and requires hundred of thousands instructions in order to calculate its output. On the other hand, AEDs rely on low-power and low-cost micro-controllers to operate, with their related constraints in terms of memory and speed. Even a few seconds of delay in formulating a diagnosis can have a deleterious effect on the survival chances of the patient, and on the operator's nerves which might think the device is malfunctioning in case it takes too long in providing a feedback. Because of the current high interest of neural networks, the embedded scene is moving towards integrating *neural-processing* modules [88] in lower end micro-controllers so things might change in the future. However, for the time being neural networks only find application in higher end devices that make use of Field Programmable Gate Arrays (FPGAs) or high-power micro-controllers.

4.1 Shockable and non-shockable ECG rhythms

By definition a shockable rhythm is a pathological ECG rhythm for which defibrillation has the potential of having a positive effect. Conversely, a non-shockable rhythm is a non-defined ECG rhythm for which defibrillation has a negative or negligible effect.

This definition is especially important because not all the rhythms involved in SCA events are shockable rhythms. There are, in fact, some exceptions where treating SCA with defibrillation have the potential to cause more harm than the triggering condition. For instance: in cases of Electromechanical dissociation the heart has a characteristic Pulseless Electrical Activity (PEA) [89]. In a case of PEA the ECG still shows an organized electrical activity that should produce a pulse, however it does not. Another case of SCA associated with a non-shockable rhythm is asystole, which is a condition characterized by the complete absence of the heart's electrical activity.

Shockable rhythms, instead, are a very restricted group of ECG rhythms containing *Ventricular Fibrillation* (VF) and pulseless *Ventricular Tachycardia* (VT). Despite being included in the same group, the two rhythms are extremely different. While the former is characterized by a chaotic undefined ECG, the latter exhibits a peculiar organized electrical activity. In relation to VT, the residual organization is what makes particularly difficult its classification. In fact, as seen

in Chapter 1, depending on the frequency and type, which can be mono-phasic, bi-phasic, or poly-phasic; VT can show very different characteristics. Furthermore, low frequency VT are usually associated with some residual pulse, which means they should be treated as non-shockable rhythms. In conclusion, consisting in an heterogeneous group, it is not trivial to generalize shockable rhythms ECG.

4.2 Shockable rhythm recognition

To keep the set-up as simple as possible, AEDs only employ a single pair of self-adhesive electrodes. As a consequence the rhythm recognition algorithm can only rely on a lead II ECG. The reason behind the choice of this particular lead is that it allows the current to travel across the heart, while still being able to acquire an ECG signal good enough for formulating a diagnosis. For this reason, from this point any reference to ECG will be in terms of lead II.

To summarize, the shockable rhythm recognition algorithm can only operate on single lead ECGs, and it needs an extremely low rate of false positives to avoid delivering of defibrillation to healthy patients. Furthermore, since it is designed to operate on data acquired in sub-optimal condition it has to be fairly tolerant to noise and human errors such as the electrodes' inversion. Finally, the algorithm needs to be actually implementable in a system with limited resources.

Since shockable rhythms appear as ECGs with heterogeneous characteristics it is not trivial to define a generalization without first extracting a model, or representing the signal in a different way.

4.2.1 The heart as a dynamic system

The ECG of a healthy heart exhibits the behavior of an oscillator with a very characteristic pulse, and a slightly variable rhythm. Having to respond to external stimuli, the sinoatrial node regulates the heart's rate of activation by varying the rhythm. However, the pulse's shape is an intrinsic characteristic of the heart and thus it does not depends from external factors, but from the heart itself and its status. Conversely, when the heart exhibits a pathological ECG, there are alterations in both pulse and rhythm.

Van der Pol was the first to notice this oscillating behavior [90] and tried to model it through a dynamic system in the form of:

$$\ddot{v} - \alpha(1 - v^2)\dot{v} + \omega^2 v = 0 \tag{4.1}$$

which is also known as Van der Pol oscillator. Equation 4.1 represent an oscillatory system of which the resistance is a function of the elongation, where v is the ECG potential in function of time, and α is a scalar parameter that represent the non-linearity and the strength of the damping.

When α is positive, the system has a resistance which for a small amplitude is negative. Therefore, for $v = 0$ the system is unstable. As long as $v^2 \ll 1$, the system will leave the $v = 0$ condition in an aperiodic way. However, when $v^2 > 1$ the resistance changes sign forcing v to move back towards the value $v = 0$. In this way after a few oscillation the system enters a characteristic cycle known as *limit cycle*, which strongly depends on the damping factor α.

Figure 4.1 depicts a Van der Pol oscillator in time domain (on left), and its phase space (right) in terms of its amplitude and the first derivative.

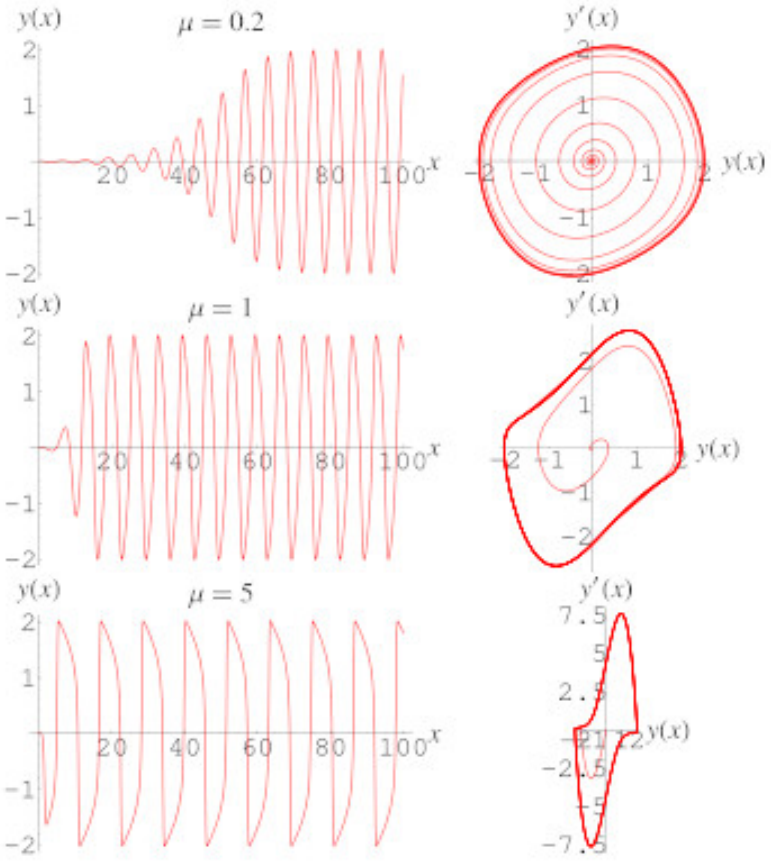

Figure 4.1: Van der Pol oscillator with different damping factors [91].

4.2.2 Time delay method

Although it can be used to model the sinoatrial node functioning, the Van der Pol oscillator is too simple to model the heartbeat as a whole. However, following the reasoning of modeling the heartbeat as an unknown dynamic model with a limit cycle, it is possible to apply Taken's theorem in order to obtain a phase space representation of the ECG.

A phase space is an abstract space, which graphically represents the states of a dynamic state. The dimension of the phase space is equal to the number of variables required to describe completely the state of the system. However, if the actual number of variables governing a dynamic system is not known, the phase space can be reconstructed with Taken's theorem, also known as the time-delay embedding theorem [92].

Taken's theorem states that if the dynamics of a system are governed by a certain number (d) of independent variables, say x_i; but only one, say y, is accessible; then it is possible to reconstruct the system's dynamic from the single observed variable y by plotting in a phase space its values against itself for a certain number k of times at a predefined time delay τ. Furthermore, the embedding dimension k is at most $2d + 1$. Equation 4.2 describes formally Taken's theorem where X is the vector containing the reconstructed phase space.

$$X = \begin{bmatrix} x_1 \\ x_2 \\ \vdots \\ x_{n-(d-1)\tau} \end{bmatrix} = \begin{bmatrix} y_1 & y_{1+\tau} & \cdots & y_{1+(d-1)\tau} \\ y_2 & y_{2+\tau} & \cdots & y_{2+(d-1)\tau} \\ \vdots & \vdots & & \vdots \\ y_{n-(d-1)\tau} & y_{n-(d-2)\tau} & \cdots & y_n \end{bmatrix} \tag{4.2}$$

Choosing an appropriate value τ and d is fundamental as the whole process depends on those two parameters. If the dimension is too low the phase space is not capable of effectively reconstructing the system, if it is too high the representation will be pointlessly complicated. On the other hand, τ should have a convenient value to incorporate the dynamic of the attractor.

It is possible to apply Taken's theorem to the ECG problem. In this case the dynamic system is the heart, which is governed by an unknown number d of independent variables x_i, whilst only the lead II ECG can be observed (y). However, the problem of chosing an appropriate d and τ still remain open. For the sake of simplicity, the proposed solution employs a dimension of the reconstructed phase space $d = 2$. For what it regards τ, the inherent rhythmicity of the ECG was exploited in order to set τ equal to the demi-period of a heartbeat. Figure 4.2 shows two examples of ECG signals and their respective phase space reconstruction. The phase space allows to represent the signal by its limit cycle, which is relatively easy to discriminate between shockable and non-shockable rhythms, as Figure 4.2 proves.

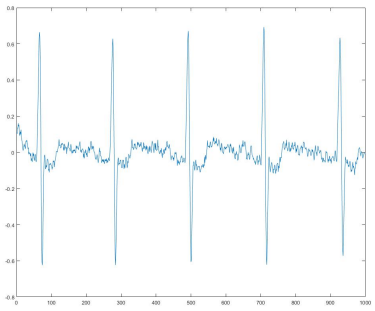

(a) ECG of a Normal Sinus Rhythm (NSR).

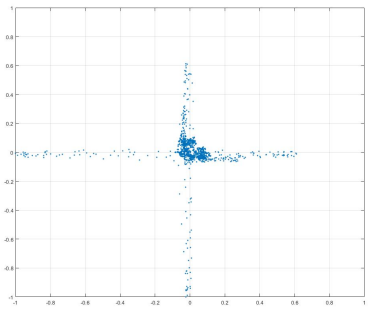

(b) Bi-dimensional phase space reconstruction of the NSR ECG.

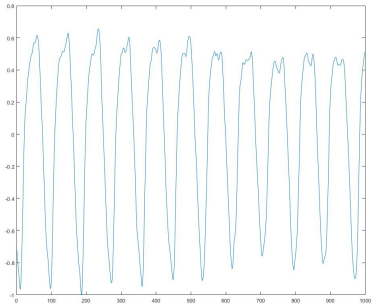

(c) ECG of a mono-phasic Ventricular Tachycardia (VT) rhythm.

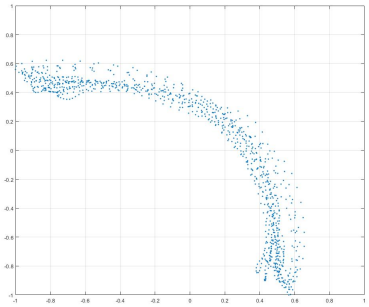

(d) Bi-dimensional phase space reconstruction of the mono-VT ECG.

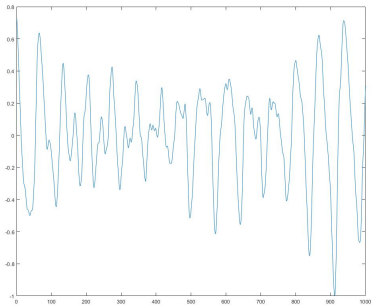

(e) ECG of a poly-phasic Ventricular Tachycardia (VT) rhythm.

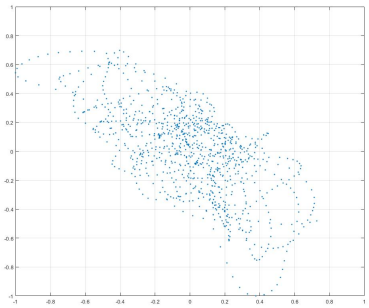

(f) Bi-dimensional phase space reconstruction of the poly-VT ECG.

Figure 4.2: Bi-dimensional phase space reconstruction of lead II ECG signals.

4.2.3 Autocorrelation based time delay

In the last section it was showed how the reconstructed phase space of an ECG can be used to highlight differences between shockable and non-shockable rhythms,

in terms of limit cycles. However, last section leaves open the problem of finding the demi-period of the signal in order to properly adjust the value of τ.

The autocorrelation is formally defined as the correlation of a signal with a delayed copy of itself as a function of such delay. Given a discrete signal $x(n)$, the autocorrelation function can be expressed in terms of delay l as:

$$R_{xx}(l) = \sum_{n \in Z} x(n)x(n-l) \tag{4.3}$$

High values of R_{xx} at a given l can be interpreted as a repeating pattern with cadence $1/l$, while low negative values can be interpreted as anti-pattern. Evaluating the local maxima of the absolute value of the autocorrelation it is possible to find the periods of inherent patterns inside a signal.

In other words: the autocorrelation function can be used to find repeating patterns in a time series, and therefore can be exploited to find the period of an ECG signal.

What makes autocorrelation so interesting with regards to other techniques used to evaluate the heart-rate such as the Pan-Thompkins algorithm [93]; is that according to the Wiener-Kuinchin theorem it can be evaluated as the inverse fourier transform of the Power Spectral Density (PSD) function of a signal [94]. The PSD, as explained later, is required to differentiate VT from VF, therefore estimating R_{xx} is convenient in this specific problem.

4.2.4 K-Means

The phase space reconstruction technique described earlier in this chapter offers a convenient representation for ECGs in terms of their limit cycle. If the ECG is modeled as an oscillator, and the limit cycle represents the stability state of the oscillations, it is reasonable to expect that different limit cycles represent different oscillations, and thus different rhythms. In particular, mono- and bi-phasic VT are characterized by an highly symmetrical pattern that repeats itself at a high frequency. On the other hand, polymorphic VT and VF are characterized by a chaotic dynamics, which will appear differently in the phase space. Conversely, a Normal Sinus Rhythm (NSR) is characterized by a repeating non-symmetrical pattern, which is represented by a characteristic cross in the phase space. All other non-shockable rhythm alteration are represented as slight variation on the pattern and frequency of the NSR oscillation, thus appearing similar to NSR in the phase space. However, so far it is still missing a generalization for the discrimination between non-shockable and shockable rhythms.

In the proposed solution, K-Means [95] is exploited to reduce the cluster of points in the phase space to a more compressed representation. K-Means is a clustering method used to represent different clusters of an observation with their nearest centroid. The resulting centroid can then be used to represent the cluster

for further analysis. Given a sequence of n observations $X = (x_1, x_2, \ldots, x_n)$, the K-Means method goal is to partition X in $k \leq n$ clusters $C = (C_1, C_2, \ldots, C_k)$ in order to minimize the within-cluster sum of square:

$$\arg\min_{C} \sum_{i=1}^{k} \sum_{x \in C_i} \|x - \mu_i\|^2 = \arg\min_{C} \sum_{i=1}^{k} |C_i| \operatorname{Var} C_i \tag{4.4}$$

where μ_i represent the mean of the points in C_i.

Lloyd's algorithm

Despite K-Means is a inherently difficult problem to solve computationally, there are various efficient heuristic algorithms that converge quickly to a local minimum. For the sake of simplicity the proposed approach employed the Lloyd's algorithm [96] in order to estimate C_i. In the Lloyd's algorithm, also known as naive approach, the centroids are found by alternating between two steps. The first step is the assignment, in which each observation is assigned to the nearest cluster:

$$C_i^l = \left\{ x_p : d(x_p, m_i^l) \leq d(x_p, m_j^l) | \forall j, 1 \leq j \leq k, j \neq i \right\} \tag{4.5}$$

where $d(x, m)$ is the distance function, and m^l represents the centroids position in the iteration l.

The second step is called update step and consist of recalculating the centroids position based on the new assignment:

$$m_i^{(l+1)} = \frac{1}{C_i^l} \sum_{x_j \in C_i^l} x_j \tag{4.6}$$

Despite this algorithm does not guarantee to find the optimum solution, it will converge in a fairly reasonable amount of iteration. The convergence condition is that the assignment does not change for more than a certain amount of points.

Distance function

Because of the problem's geometric symmetries along the phase space's axes, the distance function has been implemented with a Manhattan distance. In the Manhattan distance, also known as taxicab metric, distances between two points p_1 and p_2 is given by the sum of the lengths of the segments obtained projecting the points onto the coordinate axes:

$$d(p_1, p_2) = \|p_1 - p_2\|_1 = \sum_{i=1}^{n} |p_1^i - p_2^i| \tag{4.7}$$

where n is the dimension of the space. Consequently, in the case of a plane such as the phase space considered in the proposed solution the Manhattan distance can be expressed as:

$$d(p_1, p_2) = |p_1^x - p_2^x| + |p_1^y - p_2^y| \tag{4.8}$$

Therefore the Manhattan distance benefits axial distances over diagonal ones. In this way the cross-like shape of a NSR ECG has an advantage over any other arbitrary shape.

Algorithm implementation

In the proposed solution the convergence threshold for Lloyd's algorithm has been set as 10% of the total points. Additionally, it was implemented a safety back-up mechanism for centroids that at the end of the Lloyd iteration are stuck with no points. In such case the centroid is repositioned halfway through the centroid with most points in an attempt of redistributing the cluster.

The last two parameters to define in order to use the Lloyd's algorithm are the number of cluster k and their initial position m^0. Both k and m^0 depends on data and should be tailored according to the problem's specification. Since the time delay τ has been set to half the period of the signal, non-shockable rhythms are reconstructed in the phase space as a cross-like shape where: the center contains most of data, corresponding to the isoelectric line of the ECG; while the arms mostly represents the QRS complexes. Exploiting this peculiar shape it is possible to place $k = 5$ centroids according to this cross: one on the center, which will represent most of data; and the other four on the cross' edges, representing just a little portion of the initial data. If the reconstructed phase space has the shape of a cross, the five centroids will not be able to move since most of data is already represented by the central centroid; otherwise, if data does not have a cross-like shape, the centroids will be pushed away and data will be redistributed among all five of them. Figure 4.3 depicts the results of the proposed solution applied to the same signals showed in Figure 4.2.

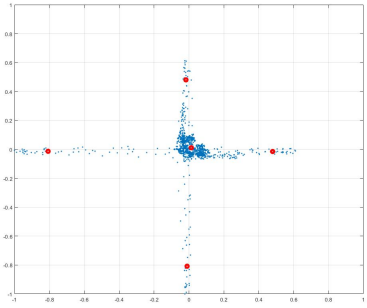

(a) K-Means method applied to a NSR ECG.

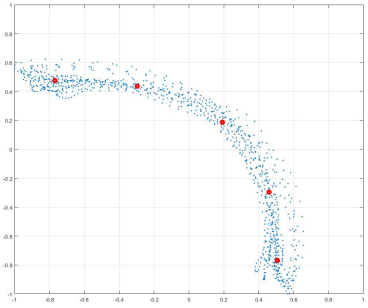

(b) K-Means method applied to a mono-VT ECG.

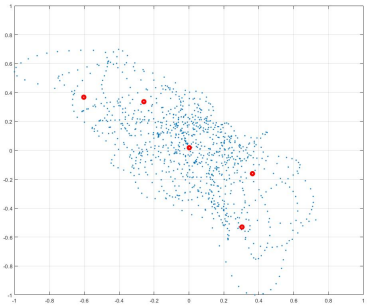

(c) K-Means method applied to a poly-VT ECG.

Figure 4.3: K-Means applied to the phase space reconstruction of different lead II ECG.

4.2.5 Links

Exploiting the K-Means method allows to reduce the problem in terms of recognizing the position of just five centroids. However, albeit knowing the position of the centroids can already be a good indication of point's distribution shape, it is not sufficient to actually describe it. For instance Figure 4.4a shows a signals with clear signs of VT. However, because of a combination of noise and inherent pattern characteristics, the K-Means method applied on the phase space reconstruction produces a cross-alike distribution of the centroids (Figure 4.4b).

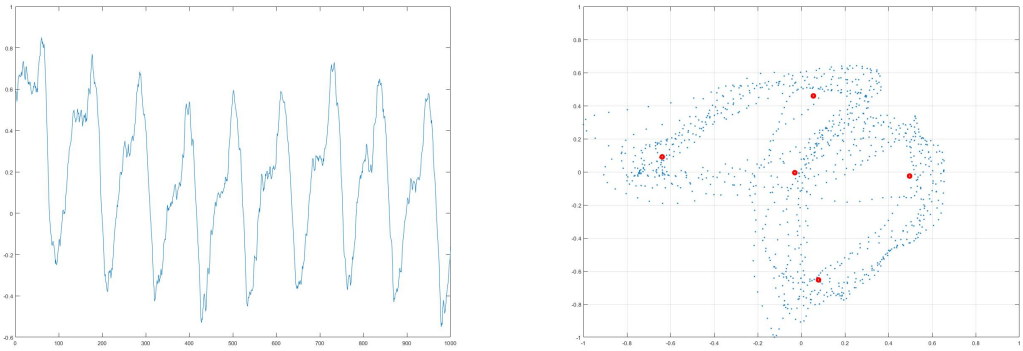

(a) Particularly noisy VT ECG.

(b) K-Means method applied to the same ECG.

Figure 4.4: K-Means applied to the phase space reconstruction of a noisy VT ECG.

Figure 4.4 highlights that use the centroids as a description of the reconstructed phase space there is still the necessity of an additional information regarding the underlying shape. In the proposed solution such information is provided in the form of links between centroids. The presence of a statistically significant amount of points between two centroids can be represented as a link among the two. Conversely the absence of a statistically significant amount of points between two centroids can be represented with the absence of a link. Therefore, a NSR ECG would appear as a cross with the four outer neurons linked with the central one; while any other configuration would appear differently. With regards to Figure 4.4b, it is clear how the left and top centroids are linked together by the presence of points.

In order to assert if two centroids C_1 and C_2 are linked, all points p_i belonging to either of the centroids are projected on a line passing between the two. If a significant amount of the projected points lay in the segment of the line enclosed by the two centroids, then a link is formed. The projection is constructed taking C_1 as the reference system, then applying a dot product between p and C_2 it is possible to obtain the distance of the projected points $d(p')_{C_1}$ with regards to C_1:

$$d(p')_{C_1} = (p - C_1) \cdot (C_2 - C_1) \tag{4.9}$$

Comparing this distance with the distance between C_1 and C_2 it is possible to assert whether a point falls within the two centroids or not. In the proposed solution the minimum amount of points to form a link was empirically set to 10% of the total points in the phase space. Figure 4.5 shows the results of the linking process applied to the signals showed in Figure 4.3 and Figure 4.4. In particular, the latter show how links play a fundamental role in the phase space points depiction.

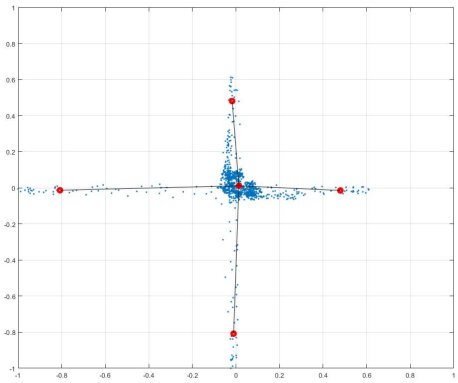

(a) NSR ECG.

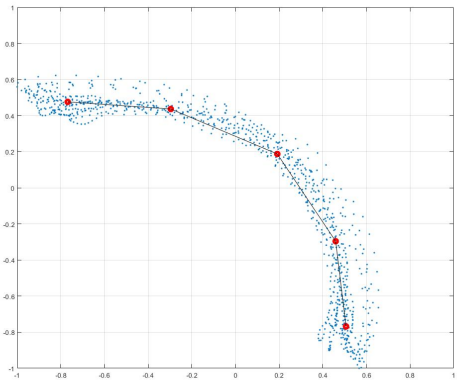

(b) Mono-VT ECG.

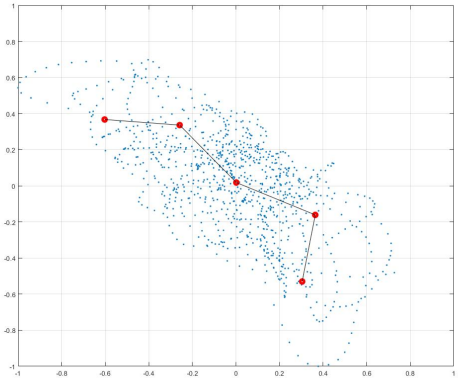

(c) Poly-VT ECG.

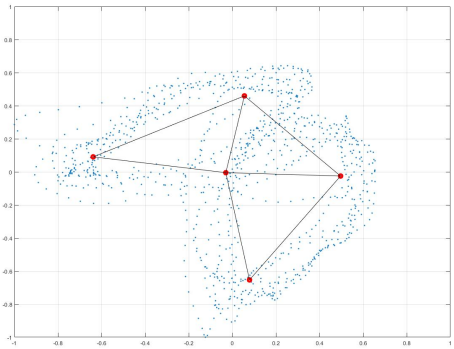

(d) Noisy VT ECG.

Figure 4.5: Linked K-Means method applied to the phase space reconstruction of different lead II ECG.

4.3 Results

Resuming, the proposed method consist of representing a lead II ECG signal in its phase space using a bi-dimensional time delay method. The phase space data is then simplified by compressing it in five representative centroids obtained applying K-Means. In order to achieve a better representation of data, the projection of points to the line intersecting two centroids was used to assert connections between coupled centroids. Finally, by controlling the resulting centroid's position combined with their connections it is possible to assert whether an ECG exhibits shockable or non-shockable rhythms. Figure 4.6 shows a NSR signal that degenerate into VT, paired with the algorithm results.

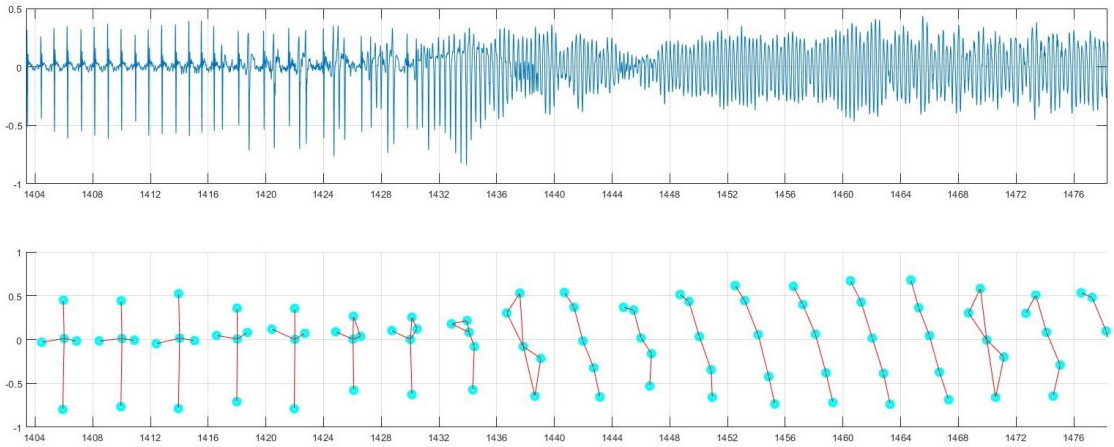

Figure 4.6: The proposed algorithm at work. On top there is an ECG, on bottom the algorithm's results.

The algorithm was implemented in Matlab to validate its performance according to the specification of IEC 60601-2-4 [97], which is a particular norm regarding "Particular requirements for the basic safety and essential performance of cardiac defibrillators". Section 201.107 of the norm describes the requirements for rhythm recognition detectors and states that the validation database shall include: VF rhythms of varying amplitudes, VT rhythms of varying rates and QRS width, and various sinus rhythms including atrial fibrillation and flutter, supra-ventricular tachycardias, sinus rhythm with premature ventricular contraction, asystole, and rhythms that includes peacemakers. Furthermore, the norm also requires that the algorithm's performance shall be expressed in terms of specificity, sensitivity, and a table reporting the results in form of Table 4.1.

Table 4.1: Algorithm results table. Template as for 60601-2-4.

	Shockable rhythm	Non-shockable rhythm
Shock	A	B
No shock	C	D

Sensitivity S_e and specificity S_p are respectively defined as:

$$S_e = \frac{A}{A+B}; S_p = \frac{B}{B+D} \tag{4.10}$$

Moreover, the norm also define the minimum value of S_e and S_p in order for the algorithm to get certified, which can be resumed as: S_p over 95% in both cases, $S_p^{VT} \geq 90\%$ for VT, and $S_p^{VF} \geq 75\%$ for VF.

The algorithm, therefore, was tested on various ECG extracted from different databases in order to satisfy the norm requirements. Signals from MIT-BIH Normal

Sinus Rhythm Database [98] (NSRDB) were used to test extensively the algorithm specificity with regards to NSR signals. The MIT-BIH Supraventricular Arrhythmia Database [99] (SVDB) was instead used to assert the algorithm specificity to supraventricular arrhythmias. Finally, the CU Ventricular Tachyarrhythmia Database [100] (CUDB) was used to assert both sensitivity and specificity to various shockable and non-shockable rhythms. Each signal was divided in events with a fixed length of four seconds, which will be the time window that the AED will have to analyze data. No further elaboration was done. Table 4.2 resumes the database composition.

Table 4.2: Test database composition.

	Signal	Shockable event	Non-shockable event	Total events
NSRDB	16272	0	10000	10000
	16420	0	19250	19250
	16773	0	19250	19250
	19093	0	9500	9500
	17052	0	18750	18750
	Summary	0	76750	76750
CUDB	cu01	74	53	127
	cu04	75	52	127
	cu05	30	97	127
	cu13	18	109	127
	cu17	10	117	127
	cu22	28	99	127
	cu32	12	115	127
	cu24	17	110	127
	Summary	264	752	1016
SVDB	801	0	450	450
	820	0	450	450
	842	0	450	450
	858	0	450	450
	883	0	450	450
	Summary	0	2250	2250

Finally, the test results are resumed in Table 4.3 in terms of: true positive TP, true negative TN, false positive FP, false negative FN, and the resulting sensitivity S_e and specificity S_p. It is important to note that most of these recordings were containing noise, which according to 60601-2-4 have to be removed. However, in order to test the algorithm in the worst case scenario it was decided not to alter data.

Table 4.3: Test results.

	Signal	TP	FP	FN	TN	S_e [%]	S_p [%]
NSRDB	16272	0	0	0	10000	0	100.00
	16420	0	0	0	19250	0	100.00
	16773	0	0	0	19250	0	100.00
	19093	0	0	0	9500	0	100.00
	17052	0	0	0	18750	0	100.00
	Summary	0	0	0	76750	0	100.00
CUDB	cu01	74	0	0	53	100.00	100.00
	cu04	72	0	3	52	96.00	100.00
	cu05	28	0	2	97	93.33	100.00
	cu13	17	0	1	109	94.44	100.00
	cu17	10	0	0	117	100.00	100.00
	cu22	27	0	1	99	96.43	100.00
	cu32	12	0	0	115	100.00	100.00
	cu24	17	1	0	109	100.00	99.09
	Summary	257	1	7	751	97.34848	99.87
SVDB	801	0	0	0	450	0	100.00
	820	0	0	0	450	0	100.00
	842	0	1	0	449	0	99.78
	858	0	0	0	450	0	100.00
	883	0	0	0	450	0	100.00
	Summary	0	1	0	2249	0	99.96
Final score		257	2	7	79750	97.34848	99.99749

4.4 Discriminating VT from VF

In conclusion of this chapter there is still an important distinction to do among shockable rhythms. In fact, as stated in the introduction low frequency VT are usually associated with a pulse. Therefore, after a shockable rhythm has been recognized a final check should assert whether the rhythm is VT or VF, and in case it is VT with a low frequency the rhythm should be recognized as non-shockable. As a reference, low frequency in terms of VT is defined for less than 150 bpm.

Despite being recognized both as shockable rhythm, VT and VF exhibits a rather different behavior. VT, in fact, follow a highly organized pattern; while VF has a chaotic disorganized behavior. As a results it is reasonable to expect that the Power Spectral Density distribution for VT and VF is rather different. In fact,

VT exhibits a PSD marked by a very narrow band, as shown in Figure 4.7b; while VF has a more distributed energy content. The evaluation of the PSD function has been explained in chapter two in Equation 2.2.

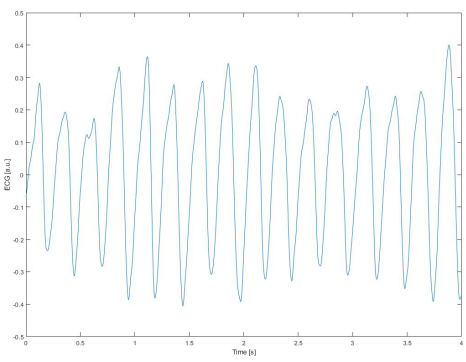

(a) VT ECG.

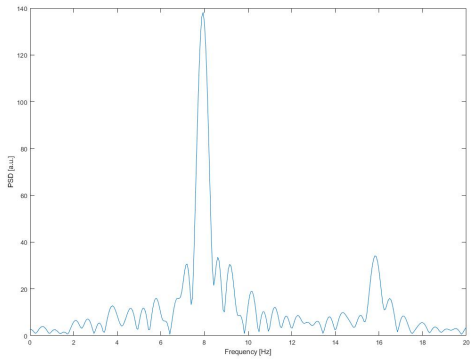

(b) VT PSD.

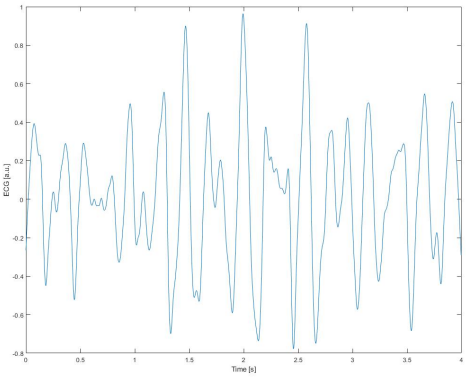

(c) VF ECG.

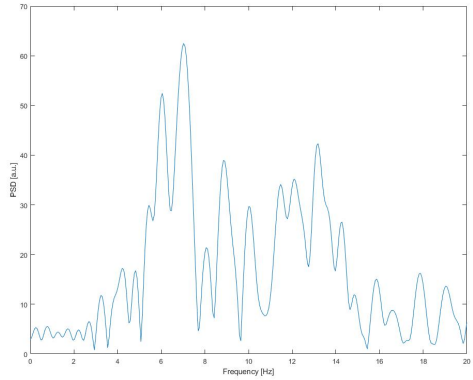

(d) VF PSD.

Figure 4.7: Differences between VT and VF Power Spectral Distribution.

As a result, it is possible to use the Cumulative Spectral Power (CSP) described in Equation 2.3 in order to differentiate VT from VF setting a narrow bandwidth for the higher and lower bounds.

Chapter 5

Development of an Automated External Defibrillator

In chapter 2 it was presented a series of wearable devices with ECG acquisition capabilities, after which chapter 3 introduced a novel approach on the ECG classification problem. Since chapter 4 dealt with shockable rhythm recognition algorithms to be implemented in Automated External Defibrillators (AED), the only logical conclusion this dissertation is to present a novel device that implements the algorithm presented in chapter 3.

In principle an AED is a rather simple device. A micro-controller has to manage the charge and consequent discharge of a capacitor in response to the detection of a shockable rhythm. Albeit the previous is an obvious understatement contrived to conceptualize a complex device, it is not so far from reality. In fact, what makes complicated an AED is a combination of multiple factors, first of which the presence of a high-voltage circuitry operating back-to-back with delicate electronics such as the ECG analog front-end. Furthermore, being a medical device, an AED has to offer not only an absolute and categorical safety of operation, but has also to be able to provide accurate forensic information regarding each and every use in case something unexpected happens. As a matter of fact, the ECG file produced during the use of an AED can be used as a evidence in case of litigation, e.g. to prove that there was actually an attempt in resuscitating a SCA victim. Moreover, being used primarily by under-trained operators in stressful conditions, an AED should provide some error-tolerant behavior as well as to guide the user in each step by means of voice commands and visual feedback. All these functions, and many more, combined together in a reasonably small, inexpensive, and low power device; makes the design process of an AED a rather complicated task.

The scope of this chapter, however, is not to provide a guide or a rationale on the design process of an AED. As a matter of fact, the author already discussed about it in [101] and in [102]. Instead, here will be presented a novel device that was expressly designed to operate with the algorithm showed in chapter 4 to act

both as a benchmark and as a link between the research's and consumer's worlds.

5.1 Hardware description

The proposed AED's block diagram is showed in Figure 5.1, where every element is grouped depending on the physical PCB it belongs. The system has two main boards: the high-voltage board, represented by the top red group; and the control-board, represented by the bottom yellow group. The two main boards are matched with three or four satellite boards depending on the configuration. The extra board is required for the display operation. Despite technically it is not part of the device, the battery board was included in the block diagram because, for obvious reason, the system cannot work without it.

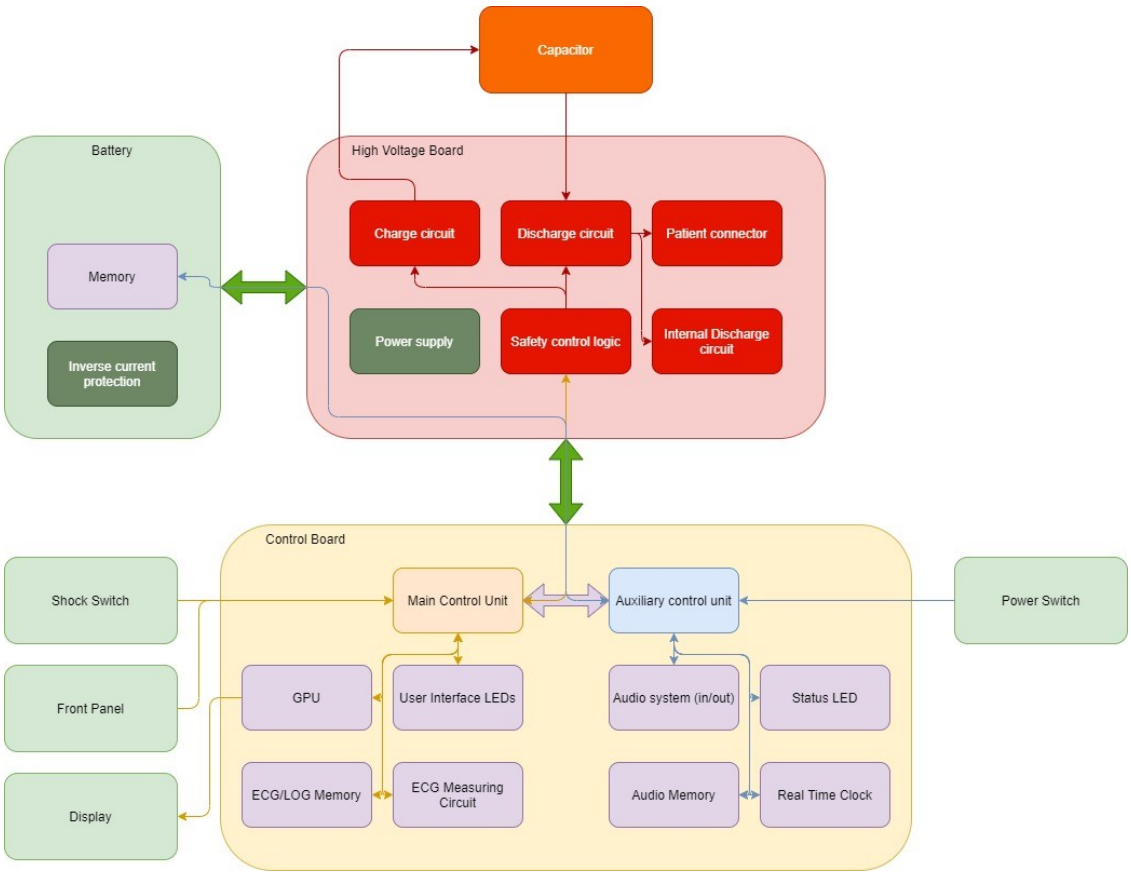

Figure 5.1: The AED block diagram.

Starting from the battery: besides the $LiMnO_2$ cells, the battery-pack contains a PCB populated with some protection circuitry and a EEPROM memory. The memory is required to save important information about the evolution of the

State of Charge (SoC) of the battery. Accurate estimations of the battery's SoC is indeed of vital importance for the correct operation of the device. In fact, the consequences of the AED shutting down during its operation can have unpredictable results, where in the best case scenario the device simply won't turn on and the patient chances of survival drop significantly. Since $LiMnO_2$ cells have a rather flat Voltage-SoC characteristic, SoC estimation is an intrinsically difficult problem that require different parameters such as: temperature, currents, and internal impedance estimation. The time evolution of such parameters is saved in the internal memory of the battery. In this way the SoC can be estimated even if the battery is removed and placed on other devices.

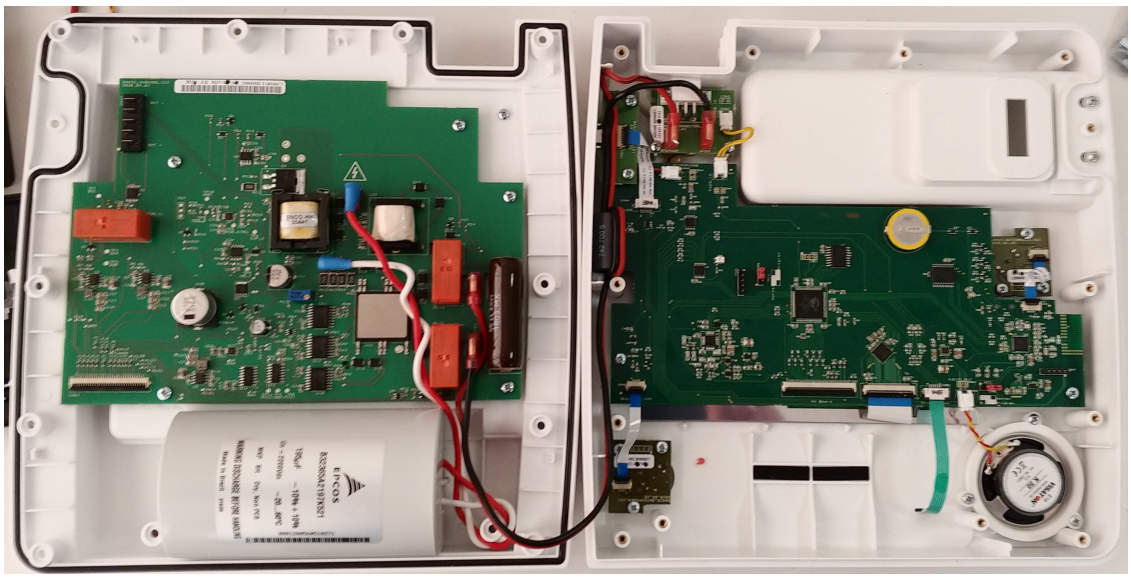

Figure 5.2: The AED as seen from the inside. Left side is the high-voltage board, right side is the control board.

The high-voltage board contains all the circuitry that safely controls the charge and discharge of the defibrillation capacitor. The charging circuit is a relatively high-powered DC-DC converter that, starting from the $12V$ provided by the battery, can charge the capacitor to a voltage up to $1850V$ in less than 8 seconds. The discharge circuit, instead, consist of a IGBT H-Bridge that allows biphasic discharges in the patient. Additionally, in cases when the capacitor is charged, but for some reason the defibrillation is no longer required, e.g. the electrodes were disconnected; the high-voltage board is also equipped with an internal discharge circuit, consisting of a $25W$-50Ω resistor perfectly capable to absorb all the capacitor residual energy. Finally, the high-voltage board includes protection circuitry to protect it in case of misuse or faulty conditions. These protections includes, but are not limited to: over-current protection on the charging circuit, over-voltage protection on the capacitor, and short-circuit protection on the discharge circuit in both

terms of: H-Bridge phases, and electrodes shorting. Finally the high-voltage board also incorporates the DC-DC converters required to power all AED's circuitry.

Finally, the control board contains the AED's brain with all the related electronics. From a functional point of view the control board can be divided in two parts: the main control unit (MCU), and the auxiliary control unit (ACU). MCU is the responsible of the most important operations during the active use of the device and some of its most important tasks include: controlling the high voltage circuitry; acquiring, analyzing, and storing the ECG and impedance signals; saving detailed logs of operation; managing the user-machine interactions; etc. The ACU, instead, is mostly responsible of the stand-by operation of the device waking-up the MCU when it is required, monitoring the battery, and keeping track of time. Besides the stand-by operations, however, ACU is also responsible for the audio system in terms of both performing ambient recordings and producing an audio signal when MCU requires it.

5.2 Mode of operation

The AED operation is organized as a Finite State Machine (FSM) with twelve distinct states, where each state is characterized by different operative and logical conditions. Each state is in turn organized as three different parts that defines its life cycle: init, loop, and exit. The state's init is the early stage of the state, where the FSM correctly initializes the resources required for the state's operation. The loop stage, instead, represents the permanent functioning of the state, from which it is only possible to exit after the occurrence of certain events depending on the state itself. Finally, the exit stage represents the state's end of life, which is responsible for the correct release of the resources used by the state operation as well as the selection of the state that will follow the current one.

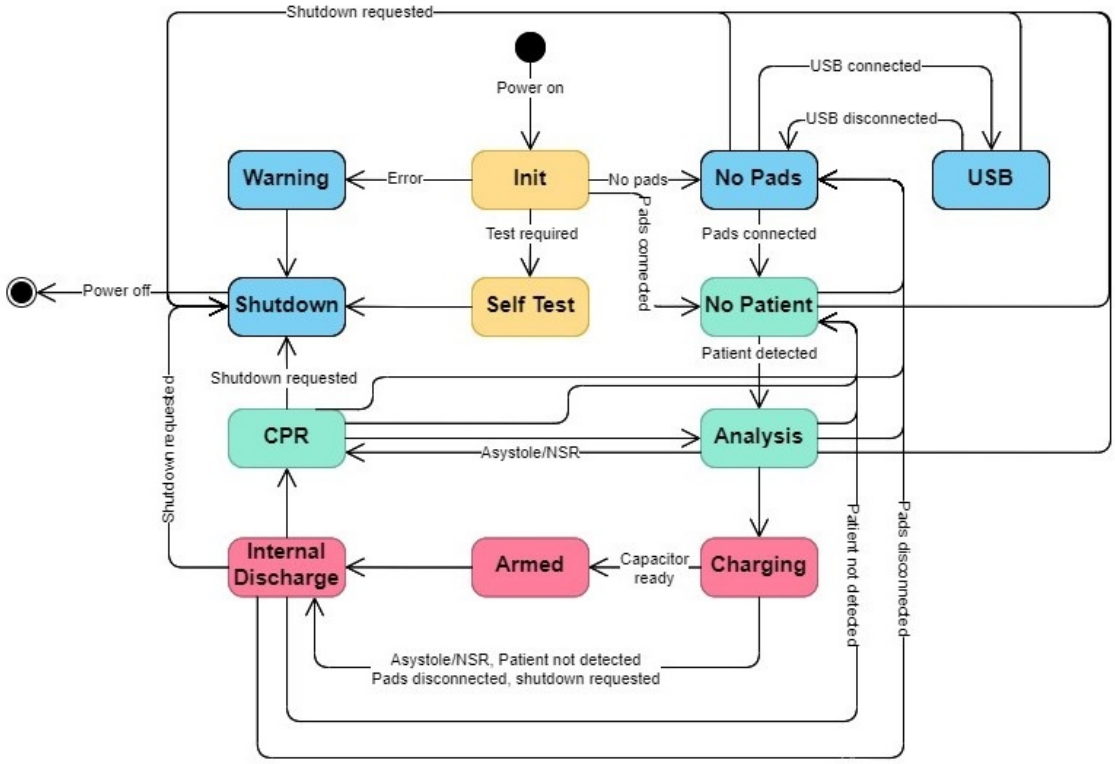

Figure 5.3: AED mode of operation: a twelve states finite state machine.

Figure 5.3 represents a simplified version of the 12-state FSM with a color-code based on the state's capability of operating the high-voltage circuitry, or interacting with the patient in terms of ECG, impedance, or defibrillation. In this, yellow-colored states are those which can control the high-voltage circuitry, but cannot interact with the patient. Red states, instead, not only can operate the high-voltage circuitry, but can also interact with the patient. Conversely, green states can interact with the patient, but cannot control the high-voltage circuit. Finally, blue states have no mean of interacting with the patient and no access to the high-voltage circuitry.

What follows is a brief description of the functioning of some of the most important states, which allow a better understanding on how the device operates.

5.2.1 State: Analysis

When in this state, the AED performs ECG acquisitions and formulates a diagnosis in order to decide whether the patient requires defibrillation or not. In order to enter in this state it is required that the pads are correctly placed on a patient. In this state the high-voltage circuitry is disabled.

Init

During the analysis state initialization the device checks if the pads are actually connected to a patient by analyzing the impedance. After that, the operator will be warned not to touch the patient in preparation of the upcoming rhythm analysis. Consequently, when the message is over, the device wait up to four more seconds in order to give the operator enough time to stop interacting with the patient.

Loop

During the analysis loop the system continuously perform three fundamental checks:

1 the occurrence of an asynchronous request of changing state, e.g. the operator pushing the shutdown button.

2 the patient's impedance, which determines the premature exit from the state in case the AED cannot detect anymore the patient.

3 ECG data is ready to be analyzed. In this case the system will perform post-processing operations on the data, followed by the application of the algorithm described in the previous chapter. Depending on the result of the algorithm, this analysis can be repeated up to three times in case of non-shockable rhythms.

Exit

The exit from this state does not require particular operations.

5.2.2 State: Armed

This state is entered when the system is ready to deliver a defibrillation discharge to the patient.

Init

Upon entering this state the AED will enable the defibrillation button and starts emitting a sound alarm.

Loop

This state implements a variation of the *Analysis* loop in which the condition 3 is repeated up to three times until the patient exhibits a **shockable** rhythm. Moreover a fourth check is made on the defibrillation button. In case it is pressed the AED will deliver the shock and exit the state right away.

Exit

Upon exiting this state the AED will disable the shock button as well as stopping the sound alarm.

5.2.3 State: Charging

The charging state is analogous to the *Analysis* state, with the only difference that the capacitor is charging.

Init

Entering this state causes the charging circuit to be activated in conjunction with the charging sound alarm.

Loop

The loop is similar to the one of the *Armed* state, with the difference that the fourth check is on the capacitor state: when it reaches the desired voltage a change of state is requested.

Exit

When exiting from this stage the charging sound alarm is stopped.

5.2.4 State: Self-test

This special state allows the machine to perform a diagnostic check on the main components in order to avoid malfunctions.

Init

Upon entering this state the AED will enable the shock button, requesting the operator to push it in order to perform the tests.

Loop

During the loop, the AED will wait up to 15 seconds for the operator to push the button. When the button is pressed the device will perform a series of diagnostic tests to evaluate the device state. These tests include: high-voltage charging and discharging, ECG tests, memory access tests, pads recognition tests, date/time tests, etc.

Exit

Exiting this state the device will provide a feedback on the test's results to the operator.

5.3 Tests

This device was designed with the fundamental requirement of implementing the novel algorithm described in chapter 4. For this purpose, the AED acted as a benchmark for the validity of a real-world implementation of the proposed algorithm to assert both the performance of the results and the computational efficiency.

The results were evaluated with the aid of a defibrillator analyzer: the Fluke 7000DP [103]. This is a high-performances analyzer that, among other functions, can simulate a patient by providing a variable ECG waveform that can be recognized by the AED. Moreover, in case of a shockable rhythm the analyzer can be used to assert the defibrillation quality in terms of energy accuracy and defibrillation waveform, as shown in Figure 5.5.

Figure 5.4: AED test configuration.

During the AED tests, each available waveform was evaluated with regards to the expected output for a duration of time sufficient to analyze each rhythm not less than three times. Figure 5.4 shows the actual test configuration.

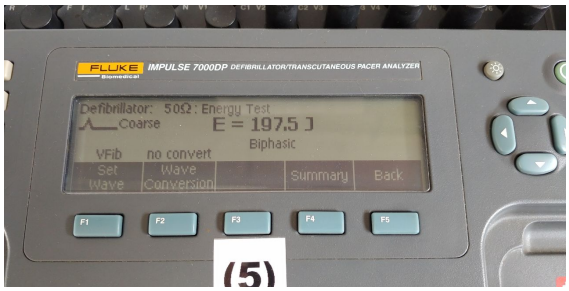

Figure 5.5: AED defibrillation test results.

The results are presented according to Table 4.1 in Table 5.1. The AED was capable of correctly recognizing all the different waveform tested with the defibrillator analyzer. The average elaboration time for the algorithm was around 1.5 seconds, which is overall an acceptable delay with regards to an acquisition window of four seconds.

Table 5.1: Algorithm results in terms of Sensitivity and Specificity.

	Signal	A	B	C	D	S_e [%]	S_p [%]
7000DP	Shockable	60	0	0	0	100.00	100.00
	Non-shockable	0	0	0	90	100.00	100.00
	Summary	60	0	0	90	100.00	100.00

Chapter 6

Conclusions

Sudden Cardiac Arrest (SCA) is a deadly condition in which the heart unexpectedly stops beating in a functional manner, thus effectively stopping the patient's blood flow. When this happens the patient can only survive if the blood's flow is promptly restored by restarting the heart's activity, e.g. with defibrillation; or by artificially forcing the flow, e.g. with Cardio-Pulmonary Resuscitation (CPR). What makes especially deadly SCA, besides requiring immediate action, is that the underlying causes can remain silent for years until the fatal event. Therefore, the only effective weapons to fight SCA are preventive screenings, and a readily available Automated External Defibrillators (AED). However, preventive screenings can only be effective when performed with regular cadence. In addition, rare events are difficult to spot unless the exams contemplate long-lasting investigations. On the other hand, although AEDs are a life-saving commodity, they cannot be seen as a definitive solution to the problem. As a matter of fact, AED can only *rise* the chance of survival during a SCA event, and not ensure it. For this reason, AEDs should aim have the best achievable performances, especially in terms of response time. In particular, during the rhythm analysis AEDs require that the rescuer does not touch the patient. As a consequence, the longer the analysis takes the longer the patient will suffer hypoxia, and thus if the rhythm recognition fails, the patient not only missed their chance of being defibrillated, but also had delayed CPR for all the duration of the analysis drastically lowering the rate of survival.

6.1 Achieved results

The main goal of this dissertation was to provide a contribution to the above-mentioned problems by supplying a new sets of instruments that could be employed in fighting arrhythmias both before and after an SCA event.

To summarize, the main contributions are:

- a series of low-cost wearable devices capable of ECG and PPG acquisitions

that can be employed to frequently monitor the heart in order to spot early signs of arrhythmias;

- an innovative arrhythmia classifier that analyzes ECGs using 1D-CNN;
- a novel approach to shockable rhythm recognition by exploiting K-Means clustering in a reconstructed phase space;
- a new fully-fledged AED that efficiently employs the shockable rhythm recognition algorithm to provide diagnosis with the least amount of delay possible.

These accomplishments were confirmed with a series of experiments that yielded the following results:

- ECG signals whose quality and heart-beat estimation are compatible with consolidated medical gold standards can be obtained from *ECG Watch* and *Vital ECG*;
- *PulsECG*'s synchronous ECG and PPG acquisitions yields an ECG signal qualitatively comparable with those obtained with the above-mentioned devices;
- proof that 1D-CNN can be used to assert arrhythmias, provided that the starting dataset is consistent and balanced;
- evidence that deep networks can extract and further abstract the same temporal-like attributes that humans employ in feature engineering;
- employing K-Means in describing shapes of the ECG phase space reconstructions produces results with very high rates in terms of sensitivity and specificity;
- the new AED efficiently implements the novel algorithm, and obtained the CE marking.

6.1.1 Wearable ECG devices

The first step towards arrhythmias recognition is to form an in-depth knowledge of the ECG signal. In Chapter 2 a series of wearable low-cost devices with ECG capabilities were presented and discussed. Such devices could have a profound impact on heart diseases' prevention because they would open to a large consumer audience the chance to perform self check-ups that nowadays only specialized centers allow. The ECG recordings produced by wearable devices can then either be sent to specialists, or analyzed with automated algorithms. Regardless of how data is handled, these devices can provide an improved way of spotting early signs of

cardio-vascular diseases, or even a mean of keeping under control an existing condition. Three novel tools: ECG Watch, Vital ECG, and PulsECG; are presented with an in-depth description of the design and validation process. In particular, the former two were compared with two different professional-grade CE certified electrocardiograph; while the latter was only analyzed qualitatively because of the limitation imposed by the COVID-19 pandemic. This comparison highlighted that, despite the gold standards are obviously capable of better performances, the ECG obtained with both ECG Watch and Vital ECG has compatible characteristics in terms of quality and heart-rate estimation. Furthermore, qualitatively speaking PulsECG seems capable of extracting ECG signals compatible with the other two devices, with the addition of providing a synchronized PPG signal. In conclusion, these devices represent a valuable tool for monitoring the ECG.

6.1.2 Arrhythmia pattern recognition

The desirable rise of consumer devices with ECG capabilities described in Chapter 2, however, would produce an unmanageable amount of data that only trained physician could understand. Indeed, an ECG without interpretation is just a scribble on a paper. As a consequence, the progress on the hardware of wearable ECGs has to be paired with a similar progress on rhythm recognition algorithms, otherwise there is a concrete risk of not having any benefit whatsoever in the use of such devices. For this purpose, chapter 3 introduces the use of 1D-CNN in ECG arrhythmia recognition. At first, the technique was applied to a wide generalized problem where the network aimed at recognizing 16 different arrhythmias. However, because of class imbalances on the starting dataset, the network only succeded in recognizing some of them. A second more successful attempt was made with a less generalized approach that aimed on recognizing only 5 different arrhythmias. The results of this second network showed that a classification was indeed possible as long as the training dataset allowed it. To conclude the chapter, two more network were used to assert the inner functioning of deep networks. For this purpose intermediary outputs of the net were compared with manually-picked temporal features in terms of cross-correlation. The results proved that the 1D-CNN was indeed extracting some of the temporal features in the first layer hinting that the further abstraction of such features in subsequent layers is responsible for the good classification accuracy.

6.1.3 Shockable rhythm recognition for AED

Despite their fascinating results, deep network are still far too computationally expensive to be employed in commercial AEDs. Being constrained by memory and speed limits, the micro-controllers commonly employed in AEDs put some restrictions to the algorithm that they can implement. Furthermore, since shockable

rhythms appear as ECGs with heterogeneous characteristics it is not trivial to define a generalization without first extracting a model, or representing the signal in a different way. Another way of representation for the ECG was presented in chapter 4, where it was described how to reconstruct the phase space of a dynamic system by means of time-delay embedding. Shockable and non-shockable rhythm exhibits two very different dynamics, so the reconstructed phase space is inherently dissimilar. By exploiting K-Means clustering geometric proprieties it is possible to represent all the points in a phase space by just five centroids. In addition, it is possible to add links between paired centroids depending on the presence or absence of data between them. The combination of the centroid's position and their links, finally, is sufficient to faithfully represent shapes in the phase space complex enough to formulate a diagnosis on the rhythm. Finally, the PSD can be analyzed to discriminate VT from VF, so that low frequency VT is recognized as a non-shockable rhythm.

6.1.4 Development of an AED

In conclusion of this dissertation, Chapter 5 briefly presents a novel AED especially developed to take advantage of the shockable rhythm recognition algorithm presented in Chapter 4. The proposed device complies with all modern standards in terms of AED performances, as well as the significant IEC 60601 norms. At the time of writing the AED is in a production-ready state, and has already obtained the CE marking.

6.2 Future pathways

In this thesis the problem of cardio-vascular diseases has been tackled from different perspectives. Despite the results of the proposed tools, there are still a great number of points left open, and many more left out from this work. Moreover, because of the COVID-19 pandemic and its secondary consequences such as the electronic components shortage had a negative impact on reaching all the objectives. In fact, besides PulsECG there was another device already designed and ready for testing, if only the components were available. Some other examples of future perspective are:

- the formal validation of PulsECG;
- testing *Net 4*, or similar 1D-CNNs, with different, more-complete datasets;
- reconstructing the ECG in a higher dimensional phase space;
- developing an AED capable of employing neural networks for the rhythm recognition problem.

Bibliography

[1] Aksana Baldzizhar et al. "Ventricular tachycardias: characteristics and management". In: *Critical Care Nursing Clinics* 28.3 (2016), pp. 317–329.

[2] Domenico Corrado and Alessandro Zorzi. "Sudden cardiac death in young people and athletes". In: *Italian Journal of Medicine* 12.2 (2018), pp. 74–87.

[3] Karin Bille et al. "Sudden cardiac death in athletes: the Lausanne Recommendations". In: *European Journal of Preventive Cardiology* 13.6 (2006), pp. 859–875.

[4] Florian Egger et al. "FIFA Sudden Death Registry (FIFA-SDR): a prospective, observational study of sudden death in worldwide football from 2014 to 2018". In: *British Journal of Sports Medicine* 56.2 (2022), pp. 80–87. ISSN: 0306-3674. DOI: 10.1136/bjsports-2020-102368. eprint: https://bjsm.bmj.com/content/56/2/80.full.pdf. URL: https://bjsm.bmj.com/content/56/2/80.

[5] *Apple Watch*. Apple. URL: https://www.apple.com/it/apple-watch-series-7/ (visited on 04/30/2022).

[6] *What the Apple Watch's FDA clearance actually means*. The verge. URL: https://www.theverge.com/2018/9/13/17855006/apple-watch-series-4-ekg-fda-approved-vs-cleared-meaning-safe (visited on 04/30/2022).

[7] *AliveCore KardiaMobile*. AliveCore. URL: https://www.alivecor.it/kardiamobile (visited on 04/30/2022).

[8] *Diagram of the human heart*. URL: https://en.wikipedia.org/wiki/File:Diagram_of_the_human_heart_(cropped).svg (visited on 04/30/2022).

[9] *Conduction system of the heart*. URL: https://commons.wikimedia.org/wiki/File:ConductionsystemoftheheartwithouttheHeart-en.svg (visited on 04/30/2022).

[10] S Serge Barold. "Willem Einthoven and the birth of clinical electrocardiography a hundred years ago". In: *Cardiac electrophysiology review* 7.1 (2003), pp. 99–104.

[11] Willem Einthoven. "The string galvanometer and the measurement of the action currents of the heart". In: *Nobel Lecture, December* 11 (1925).

[12] *ECG course on a A4 paper*. URL: https://www.ecgpedia.org/A4/ECGpedia_on_1_A4En.pdf (visited on 04/30/2022).

[13] *Einthoven's triangle*. URL: https://en.wikipedia.org/wiki/Electrocardiography#/media/File:Limb_leads_of_EKG.png (visited on 04/30/2022).

[14] *Precordial electrodes placement*. URL: https://litfl.com/ecg-lead-positioning/ (visited on 04/30/2022).

[15] Frank G Yanowitz. "Introduction to ECG interpretation". In: *LDS Hospital and Intermountain Medical Center* (2012).

[16] *Sinus Rhythm ECG*. URL: https://en.wikipedia.org/wiki/Electrocardiography#/media/File:SinusRhythmLabels.svg (visited on 04/30/2022).

[17] Peter Safar. "Cerebral resuscitation after cardiac arrest: a review." In: *Circulation* 74.6 Pt 2 (1986), pp. IV138–53.

[18] Alfred E Buxton et al. "Right ventricular tachycardia: clinical and electrophysiologic characteristics." In: *Circulation* 68.5 (1983), pp. 917–927.

[19] ROSS Brooks and JOHN H Burgess. "Idiopathic ventricular tachycardia. A review." In: *Medicine* 67.5 (1988), pp. 271–294.

[20] Demosthenes G Katritsis, Wojciech Zareba, and A John Camm. "Nonsustained ventricular tachycardia". In: *Journal of the American College of Cardiology* 60.20 (2012), pp. 1993–2004.

[21] Mark E Josephson et al. "Recurrent sustained ventricular tachycardia. 1. Mechanisms." In: *Circulation* 57.3 (1978), pp. 431–440.

[22] Bruce B Lerman et al. "Mechanism of repetitive monomorphic ventricular tachycardia". In: *Circulation* 92.3 (1995), pp. 421–429.

[23] Samuel Sclarovksy et al. "Polymorphous ventricular tachycardia: clinical features and treatment". In: *The American journal of cardiology* 44.2 (1979), pp. 339–344.

[24] Borys Surawicz. "Ventricular fibrillation". In: *The American Journal of Cardiology* 28.3 (1971), pp. 268–287.

[25] Carl J Wiggers. "The mechanism and nature of ventricular fibrillation". In: *American Heart Journal* 20.4 (1940), pp. 399–412.

[26] Regis A DeSilva et al. "Cardioversion and defibrillation". In: *American heart journal* 100.6 (1980), pp. 881–895.

[27] Derek J Dosdall, Vladimir G Fast, and Raymond E Ideker. "Mechanisms of defibrillation". In: *Annual review of biomedical engineering* 12 (2010), pp. 233–258.

[28] *AHA guidelines for CPR and ECC*. URL: https://cpr.heart.org/-/media/CPR-Files/CPR-Guidelines-Files/Highlights/Hghlghts_2020_ECC_Guidelines_English.pdf (visited on 04/30/2022).

[29] Norbert Noury et al. "Fall detection-principles and methods". In: *2007 29th Annual International Conference of the IEEE Engineering in Medicine and Biology Society*. IEEE. 2007, pp. 1663–1666.

[30] Paul Smith, Mubarak Shah, and Niels da Vitoria Lobo. "Determining driver visual attention with one camera". In: *IEEE transactions on intelligent transportation systems* 4.4 (2003), pp. 205–218.

[31] Mahdi Boloursaz Mashhadi et al. "Heart rate tracking using wrist-type photoplethysmographic (PPG) signals during physical exercise with simultaneous accelerometry". In: *IEEE Signal Processing Letters* 23.2 (2015), pp. 227–231.

[32] Eduardo Gil et al. "PTT variability for discrimination of sleep apnea related decreases in the amplitude fluctuations of PPG signal in children". In: *IEEE Transactions on Biomedical Engineering* 57.5 (2010), pp. 1079–1088.

[33] Eric B Bass et al. "The duration of Holter monitoring in patients with syncope: is 24 hours enough?" In: *Archives of Internal Medicine* 150.5 (1990), pp. 1073–1078.

[34] *AliveCore KardiaMobile 6L*. AliveCore. URL: https://www.alivecor.it/kardiamobile6l (visited on 04/30/2022).

[35] *D Heart*. URL: https://www.d-heartcare.com/ (visited on 04/30/2022).

[36] Vincenzo Randazzo, Jacopo Ferretti, and Eros Pasero. "Anytime ECG Monitoring through the Use of a Low-Cost, User-Friendly, Wearable Device". In: *Sensors* 21.18 (2021), p. 6036.

[37] Vincenzo Randazzo, Jacopo Ferretti, and Eros Pasero. "ECG WATCH: a real time wireless wearable ECG". In: *2019 IEEE International Symposium on Medical Measurements and Applications (MeMeA)*. IEEE. 2019, pp. 1–6.

[38] Eros Pasero, Eugenio Balzanelli, and Federico Caffarelli. "Intruder recognition using ECG signal". In: *2015 International joint conference on neural networks (IJCNN)*. IEEE. 2015, pp. 1–8.

[39] *TI MSP430*. URL: https://www.ti.com/microcontrollers-mcus-processors/microcontrollers/msp430-microcontrollers/overview.html (visited on 04/30/2022).

[40] *TI INA333*. URL: https://www.ti.com/product/INA333 (visited on 04/30/2022).

[41] Era Ajdaraga and Marjan Gusev. "Analysis of sampling frequency and resolution in ECG signals". In: *2017 25th Telecommunication Forum (TELFOR)*. IEEE. 2017, pp. 1–4.

[42] *HC-06*. URL: https://www.olimex.com/Products/Components/RF/BLUETOOTH-SERIAL-HC-06/ (visited on 04/30/2022).

[43] *GE B105*. URL: https://www.gehealthcare.com/products/patient-monitoring/patient-monitors/b105-and-b125-patient-monitors (visited on 04/30/2022).

[44] *IEC 60601*. URL: https://webstore.iec.ch/publication/2603 (visited on 04/30/2022).

[45] Douglas G Altman and J Martin Bland. "Measurement in medicine: the analysis of method comparison studies". In: *Journal of the Royal Statistical Society: Series D (The Statistician)* 32.3 (1983), pp. 307–317.

[46] J Martin Bland and DouglasG Altman. "Statistical methods for assessing agreement between two methods of clinical measurement". In: *The lancet* 327.8476 (1986), pp. 307–310.

[47] Richard N Youngworth, Benjamin B Gallagher, and Brian L Stamper. "An overview of power spectral density (PSD) calculations". In: *Optical manufacturing and testing VI* 5869 (2005), pp. 206–216.

[48] Vincenzo Randazzo, Jacopo Ferretti, and Eros Pasero. "A wearable smart device to monitor multiple vital parameters—VITAL ECG". In: *Electronics* 9.2 (2020), p. 300.

[49] *TI cc2640R2F*. URL: https://www.ti.com/product/CC2640R2F (visited on 04/30/2022).

[50] *HTS221 TH sensor*. URL: https://www.st.com/en/mems-and-sensors/hts221.html (visited on 04/30/2022).

[51] *MPU-9250*. URL: https://invensense.tdk.com/products/motion-tracking/9-axis/mpu-9250/ (visited on 04/30/2022).

[52] *MAX30102*. URL: https://www.maximintegrated.com/en/products/interface/sensor-interface/MAX30102.html (visited on 04/30/2022).

[53] Roy Pines Sallen and Edwin L Key. "A practical method of designing RC active filters". In: *IRE Transactions on Circuit Theory* 2.1 (1955), pp. 74–85.

[54] *GE MAC2000*. URL: https://www.gehealthcare.co.uk/products/diagnostic-cardiology/resting-ecgs/mac-2000 (visited on 04/30/2022).

[55] *Twin T notch filter*. URL: https://www.analog.com/media/en/training-seminars/tutorials/MT-225.pdf?doc=MT-225.pdf (visited on 04/30/2022).

[56] *MAXM86161*. URL: https://www.maximintegrated.com/en/products/sensors/MAXM86161.html (visited on 04/30/2022).

[57] *STEMI*. URL: https://www.ecgmedicaltraining.com/what-is-a-stemi/ (visited on 04/30/2022).

[58] HUBERT V PIPBERGER et al. "Preparation of electrocardiographic data for analysis by digital electronic computer". In: *Circulation* 21.3 (1960), pp. 413–418.

[59] Nitish V Thakor, Y-S Zhu, and K-Y Pan. "Ventricular tachycardia and fibrillation detection by a sequential hypothesis testing algorithm". In: *IEEE Transactions on Biomedical Engineering* 37.9 (1990), pp. 837–843.

[60] Eduardo José da S Luz et al. "ECG-based heartbeat classification for arrhythmia detection: A survey". In: *Computer methods and programs in biomedicine* 127 (2016), pp. 144–164.

[61] Christian Brohet, C Derwael, and R Fesler. "Automated ECG diagnosis of atrial flutter by means of wavelet transform". In: *Computers in Cardiology 1994*. IEEE. 1994, pp. 773–776.

[62] Yuki Hagiwara et al. "Computer-aided diagnosis of atrial fibrillation based on ECG signals: A review". In: *Information Sciences* 467 (2018), pp. 99–114.

[63] *Apple Siri*. URL: https://www.apple.com/it/siri/ (visited on 04/30/2022).

[64] *Microsoft Cortana*. URL: https://www.microsoft.com/en-us/cortana (visited on 04/30/2022).

[65] Elena Carlotta Olivetti et al. "Deep CNN for 3D face recognition". In: *International Conference of the Italian Association of Design Methods and Tools for Industrial Engineering*. Springer. 2019, pp. 665–674.

[66] Katie Chockley and Ezekiel Emanuel. "The end of radiology? Three threats to the future practice of radiology". In: *Journal of the American College of Radiology* 13.12 (2016), pp. 1415–1420.

[67] Agence France Presse. "Computer learns to detect skin cancer more accurately than doctors". In: *The Guardian* 29 (2018).

[68] Fabio Urbina et al. "Dual use of artificial-intelligence-powered drug discovery". In: *Nature Machine Intelligence* 4.3 (2022), pp. 189–191.

[69] *The dark side of using AI to design drugs*. URL: https://www.ft.com/content/43102ee8-bee0-4803-bc51-4a313f04d550 (visited on 04/30/2022).

[70] Xue Xu, Sohyun Jeong, and Jianqiang Li. "Interpretation of electrocardiogram (ECG) rhythm by combined CNN and BiLSTM". In: *Ieee Access* 8 (2020), pp. 125380–125388.

[71] Ulas Baran Baloglu et al. "Classification of myocardial infarction with multi-lead ECG signals and deep CNN". In: *Pattern Recognition Letters* 122 (2019), pp. 23–30.

[72] Pranav Rajpurkar et al. "Cardiologist-level arrhythmia detection with convolutional neural networks". In: *arXiv preprint arXiv:1707.01836* (2017).

[73] RR Karhe and Bhagyashri Badhe. "Heart disease classification using one dimensional convolutional neural network". In: *International Journal of Innovative Research in Electrical, Electronics, Instrumentation and Control Engineering* 6.6 (2018), pp. 88–95.

[74] Jacopo Ferretti et al. "1-D Convolutional Neural Network for ECG Arrhythmia Classification". In: *Progresses in Artificial Intelligence and Neural Systems*. Ed. by Anna Esposito et al. Singapore: Springer Singapore, 2021, pp. 269–279.

[75] Ary L Goldberger et al. "PhysioBank, PhysioToolkit, and PhysioNet: components of a new research resource for complex physiologic signals". In: *circulation* 101.23 (2000), e215–e220.

[76] George B Moody and Roger G Mark. "The impact of the MIT-BIH arrhythmia database". In: *IEEE Engineering in Medicine and Biology Magazine* 20.3 (2001), pp. 45–50.

[77] Mohammad Kachuee, Shayan Fazeli, and Majid Sarrafzadeh. "Ecg heartbeat classification: A deep transferable representation". In: *2018 IEEE international conference on healthcare informatics (ICHI)*. IEEE. 2018, pp. 443–444.

[78] Muhammad Zubair, Jinsul Kim, and Changwoo Yoon. "An automated ECG beat classification system using convolutional neural networks". In: *2016 6th international conference on IT convergence and security (ICITCS)*. IEEE. 2016, pp. 1–5.

[79] *Testing and reporting performance results of cardiac rhythm and ST segment measurement algorithms*. URL: https://global.ihs.com/doc_detail.cfm?document_name=AAMI%20EC57&item_s_key=00348334 (visited on 07/16/2022).

[80] Junaid Malik et al. "Real-time patient-specific ecg classification by 1d self-operational neural networks". In: *IEEE Transactions on Biomedical Engineering* 69.5 (2021), pp. 1788–1801.

[81] Bhekumuzi M Mathunjwa et al. "ECG arrhythmia classification by using a recurrence plot and convolutional neural network". In: *Biomedical Signal Processing and Control* 64 (2021), p. 102262.

[82] Abdelrahman M Shaker et al. "Generalization of convolutional neural networks for ECG classification using generative adversarial networks". In: *IEEE Access* 8 (2020), pp. 35592–35605.

[83] Christian Szegedy et al. "Going deeper with convolutions". In: *Proceedings of the IEEE conference on computer vision and pattern recognition*. 2015, pp. 1–9.

[84] Jacopo Ferretti et al. "Towards Uncovering Feature Extraction From Temporal Signals in Deep CNN: the ECG Case Study". In: *2020 International Joint Conference on Neural Networks (IJCNN)*. IEEE. 2020, pp. 1–6.

[85] Giansalvo Cirrincione, Vincenzo Randazzo, and Eros Pasero. "A neural based comparative analysis for feature extraction from ECG signals". In: *Neural approaches to dynamics of signal exchanges*. Springer, 2020, pp. 247–256.

[86] *How does an AED with CPR feedback work?* URL: https://www.aed.com/blog/how-does-an-aed-with-cpr-feedback-work (visited on 04/30/2022).

[87] Chu Hyun Kim et al. "The effect of automatic external defibrillator with a real-time feedback on quality of bystander cardiopulmonary resuscitation: A before-and-after simulation study". In: *Health & Social Care in the Community* 27.5 (2019), e744–e751.

[88] *Embedded ML Inference for Cortex-M Systems*. URL: https://www.arm.com/products/silicon-ip-cpu/ethos/ethos-u55 (visited on 04/30/2022).

[89] Joseph J Bocka, David T Overton, and Andrew Hauser. "Electromechanical dissociation in human beings: an echocardiographic evaluation". In: *Annals of emergency medicine* 17.5 (1988), pp. 450–452.

[90] Balth Van Der Pol and Jan Van Der Mark. "LXXII. The heartbeat considered as a relaxation oscillation, and an electrical model of the heart". In: *The London, Edinburgh, and Dublin Philosophical Magazine and Journal of Science* 6.38 (1928), pp. 763–775.

[91] *van der Pol Equation*. URL: https://mathworld.wolfram.com/vanderPolEquation.html (visited on 04/30/2022).

[92] Floris Takens. "Detecting strange attractors in turbulence". In: *Dynamical systems and turbulence, Warwick 1980*. Springer, 1981, pp. 366–381.

[93] Jiapu Pan and Willis J Tompkins. "A real-time QRS detection algorithm". In: *IEEE transactions on biomedical engineering* 3 (1985), pp. 230–236.

[94] Norbert Wiener. "The extrapolation". In: *Time Series* (1964).

[95] James MacQueen et al. "Some methods for classification and analysis of multivariate observations". In: *Proceedings of the fifth Berkeley symposium on mathematical statistics and probability*. Vol. 1. 14. Oakland, CA, USA. 1967, pp. 281–297.

[96] Stuart Lloyd. "Least squares quantization in PCM". In: *IEEE transactions on information theory* 28.2 (1982), pp. 129–137.

[97] *IEC 60601-2-4*. URL: https://webstore.iec.ch/publication/26882 (visited on 04/30/2022).

[98] A Goldberger et al. "The mit-bih normal sinus rhythm database". In: *Circulation* 101.23 (2000), e215–e220.

[99] Scott David Greenwald, Ramesh S Patil, and Roger G Mark. *Improved detection and classification of arrhythmias in noise-corrupted electrocardiograms using contextual information*. IEEE, 1990.

[100] FM Nolle et al. "CREI-GARD, a new concept in computerized arrhythmia monitoring systems". In: *Computers in Cardiology* 13 (1986), pp. 515–518.

[101] JACOPO FERRETTI. "Design of an open source AED in the framework of the UBORA project". In: (2017).

[102] Jacopo Ferretti, Licia Di Pietro, and Carmelo De Maria. "Open-source automated external defibrillator". In: *HardwareX* 2 (2017), pp. 61–70.

[103] *Fluke Impulse 7000DP*. URL: https://www.flukebiomedical.com/products/biomedical-test-equipment/defibrillator-analyzers/impulse-7000dp-defibrillator-analyzer (visited on 04/30/2022).

This Ph.D. thesis has been typeset by means of the TEX-system facilities. The typesetting engine was pdfLATEX. The document class was `toptesi`, by Claudio Beccari, with option `tipotesi=scudo`. This class is available in every up-to-date and complete TEX-system installation.